J|A|C|S
ARTICLES
Published on Web 08/29/2006

Thermally Stable Perfluoroalkylfullerenes with the Skew-Pentagonal-Pyramid Pattern: $C_{60}(C_2F_5)_4O$, $C_{60}(CF_3)_4O$, and $C_{60}(CF_3)_6$

Ivan E. Kareev,[§,#] Natalia B. Shustova,[‡] Igor V. Kuvychko,[‡] Sergey F. Lebedkin,[#] Susie M. Miller,[‡] Oren P. Anderson,[‡] Alexey A. Popov,*[,†] Steven H. Strauss,*[,‡] and Olga V. Boltalina*[,‡]

Contribution from the Institute of Problems of Chemical Physics, Russian Academy of Sciences, Chernogolovka 142432, Russia, Institute for Nanotechnology, Forschungszentrum Karlsruhe, Karlsruhe 76021, Germany, Department of Chemistry, Colorado State University, Fort Collins, Colorado 80523, and Chemistry Department, Moscow State University, Moscow 119992, Russia

Received June 4, 2006; E-mail: popov@phys.chem.msu.ru; steven.strauss@colostate.edu; ovbolt@lamar.colostate.edu

Abstract: Reaction of C_{60} with CF_3I at 550 °C, which is known to produce a single isomer of $C_{60}(CF_3)_{2,4,6}$ and multiple isomers of $C_{60}(CF_3)_{8,10}$, has now been found to produce an isomer of $C_{60}(CF_3)_6$ with the C_s-$C_{60}X_6$ skew-pentagonal-pyramid (SPP) addition pattern and an epoxide with the C_s-$C_{60}X_4O$ variation of the SPP addition pattern, C_s-$C_{60}(CF_3)_4O$. The structurally similar epoxide C_s-$C_{60}(C_2F_5)_4O$ is one of the products of the reaction of C_{60} with C_2F_5I at 430 °C. The three compounds have been characterized by mass spectrometry, DFT quantum chemical calculations, Raman, visible, and ^{19}F NMR spectroscopy, and, in the case of the two epoxides, single-crystal X-ray diffraction. The compound C_s-$C_{60}(CF_3)_6$ is the first [60]-fullerene derivative with adjacent R_f groups that are sufficiently sterically hindered to cause the (DFT-predicted) lengthening of the cage $(CF_3)C-C(CF_3)$ bond to 1.60 Å as well as to give rise to a rare, non-fast-exchange-limit ^{19}F NMR spectrum at 20 °C. The compounds C_s-$C_{60}(CF_3)_4O$ and C_s-$C_{60}(C_2F_5)_4O$ are the first poly(perfluoroalkyl)fullerene derivatives with a non-fluorine-containing exohedral substituent and the first fullerene epoxides known to be stable at elevated temperatures. All three compounds demonstrate that the SPP addition pattern is at least kinetically stable, if not thermodynamically stable, at temperatures exceeding 400 °C. The high-temperature synthesis of the two epoxides also indicates that perfluoroalkyl substituents can enhance the thermal stability of fullerene derivatives with other substituents.

Introduction

The C_s-$C_{60}X_6$ skew-pentagonal-pyramid (SPP) addition pattern is exhibited by the regioisomer most commonly observed when each of six X addends forms a σ bond with one of six different cage C atoms.[1,2] Examples of compounds with this structure include $C_{60}Br_6$,[3,4] $C_{60}Cl_6$,[5,6] $C_{60}Me_6$,[7] $C_{60}Me_5Cl$,[7] $C_{60}Ar_5Cl$,[8] $C_{60}Ar_5H$,[9,10] one isomer of $C_{60}Ph_5(OH)$,[11−13] $C_{60}(t\text{-BuOO})_4X(OH)$ (X = F, Cl, *t*-BuOO, OOH),[14] and $C_{60}(OR)_5Cl$ (R = Me, Et),[15] some of which were among the first isolable exohedral derivatives of C_{60}.[3,5] Two views of a fragment of the SPP C_s-$C_{60}Br_6$ structure[3,4] are shown in Figure S-1 (Supporting Information), and a generic $C_{60}X_6$ SPP Schlegel diagram is shown in Figure 1. Five of the X substituents are positioned on a *para*[5] (p^5) loop of five edge-sharing *p*-C_6X_2 hexagons, and the sixth substituent is positioned *ortho* to one and *meta* to two

§ Russian Academy of Sciences.
# Forschungszentrum Karlsruhe.
‡ Colorado State University.
† Moscow State University.

(1) Hirsch, A.; Brettreich, M. *Fullerenes—Chemistry and Reactions*; Wiley-VCH: Weinheim, 2005.
(2) Clare, B. W.; Kepert, D. L. *J. Mol. Struct. (Theochem)* **1995**, *340*, 125−142.
(3) Birkett, P. R.; Hitchcock, P. B.; Kroto, H. W.; Taylor, R.; Walton, D. R. M. *Nature* **1992**, *357*, 479−481.
(4) Troyanov, S. I.; Popov, A. A.; Denisenko, N. I.; Boltalina, O. V.; Sidorov, L. N.; Kemnitz, E. *Fullerenes, Nanotubes, Carbon Nanostruct.* **2003**, *11*, 61−77.
(5) Birkett, P. R.; Avent, A. G.; Darwish, A. D.; Kroto, H. W.; Taylor, R.; Walton, D. R. M. *J. Chem. Soc., Chem. Commun.* **1993**, 1260−1262.
(6) Kuvychko, I. V.; Streletskii, A. V.; Popov, A. A.; Kotsiris, S. G.; Drewello, T.; Strauss, S. H.; Boltalina, O. V. *Chem. Eur. J.* **2005**, *11*, 5426−5436.
(7) Al-Matar, H.; Abdul-Sada, A. K.; Avent, A. G.; Fowler, P. W.; Hitchcock, P. B.; Rogers, K. M.; Taylor, R. *J. Chem. Soc., Perkin Trans. 2* **2002**, 53−58.
(8) Birkett, P. R.; Avent, A. G.; Darwish, A. D.; Hahn, I.; Kroto, H. W.; Langley, G. J.; O'Loughlin, J. O.; Taylor, R.; Walton, D. R. M. *J. Chem. Soc., Perkin Trans. 2* **1997**, 1121−1125.
(9) Sawamura, M.; Iikura, H.; Nakamura, E. *J. Am. Chem. Soc.* **1996**, *118*, 12850−12851.
(10) Zhong, Y.-W.; Matsuo, Y.; Nakamura, E. *Org. Lett.* **2006**, *8*, 1463−1466.
(11) Avent, A. G.; Birkett, P. R.; Crane, J. D.; Darwish, A. D.; Langley, G. J.; Kroto, H. W.; Taylor, R.; Walton, J. *J. Chem. Soc., Chem. Commun.* **1994**, 1463−1464.
(12) Palit, D. K.; Mohan, H.; Birkett, P. R.; Mittal, J. P. *J. Phys. Chem. A* **1999**, *103*, 11227−11236.
(13) Coheur, P.-F.; Cornil, J.; dos Santos, D. A.; Birkett, P. R.; Lievin, J.; Bredas, J. L.; Walton, D. R. M.; Taylor, R.; Kroto, H. W.; Colin, R. *J. Chem. Phys.* **2000**, *112*, 8555−8566.
(14) Huang, S.; Xiao, Z.; Wang, F. D.; Zhou, J.; Yuan, G.; Zhang, S.; Chen, Z.; Thiel, W.; Schleyer, P. v. R.; Zhang, X.; Hu, X.; Chen, B.; Gan, L. *Chem. Eur. J.* **2005**, *11*, 5449−5456.
(15) Avent, A. G.; Birkett, P. R.; Darwish, A. D.; Houlton, S.; Taylor, R.; Thomson, K. S. T.; Wei, X.-W. *J. Chem. Soc., Perkin Trans. 2* **2001**, 782−786.

10.1021/ja063907r CCC: $33.50

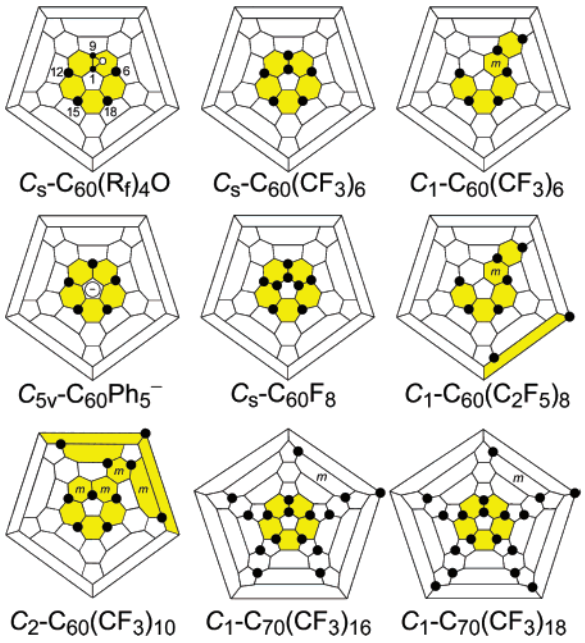

Figure 1. Schlegel diagrams for (top left to right) C_s-$C_{60}(R_f)_4O$ (R_F = CF_3, C_2F_5), C_s-$C_{60}(CF_3)_6$ (the same structure as $C_{60}Br_6$, $C_{60}Cl_6$, and $C_{60}(CH_3)_6$), C_1-p^3mp-$C_{60}(CF_3)_6$; (middle left to right) C_{5v}-$C_{60}Ph_5^-$, C_s-$C_{60}F_8$, C_1-p^3mp,p-$C_{60}(CF_3)_8$; (bottom left to right) C_2-[p^3m^2(loop)]^2-$C_{60}(CF_3)_{10}$, C_1-$C_{70}(CF_3)_{16}$, and C_1-$C_{70}(CF_3)_{18}$. Each large or small black circle denotes a fullerene C(sp^3) atom to which an O atom, a CF_3 group, or a C_2F_5 group is attached. The diagrams have been drawn to show the similarities in parts of their addition patterns, not to depict the lowest locants relative to a fixed numbering scheme. However, the numbering scheme shown for C_s-$C_{60}(R_f)_4O$ is the same as that used for C_s-$C_{60}X_6$.

of the first five. There are only a few examples of isolable $C_{60}X_6$ compounds with alternative structures, and these are $C_{60}H_6$,[16] $C_{60}F_6$,[17] $C_{60}(C(CH_3)(CO_2t\text{-Bu})_2)_6$,[18] a second isomer of $C_{60}Ph_5(OH)$,[13,19] and C_1-$C_{60}(CF_3)_6$.[20,21] The *para*^{3}-*meta*-*para* (p^3mp) ribbon of five edge-sharing $C_6(CF_3)_2$ hexagons exhibited by the latter compound can be seen in its Schlegel diagram in Figure 1.

Since 2005, the SPP pattern has also been reported for [70]-fullerene compounds. The hexakis(alkylperoxo) compound $C_{70}(t\text{-BuOO})_6$ isolated by Gan and co-workers is believed to exhibit the SPP pattern.[22] In addition, the SPP pattern is a fragment of the addition patterns of the more highly substituted [70]-fullerenes $C_{70}Cl_{16}$,[23] $C_{70}(CF_3)_{16}$,[24] and $C_{70}(CF_3)_{18}$.[24] The latter two compounds are also the first recognized examples of well-characterized fullerene$(R_f)_n$ derivatives with a pair of *ortho* perfluoroalkyl groups, which are sterically more demanding than Br atoms (and there is only *one* example of a fullerene with an *o*-C_6Br_2 hexagon).[25−27] All other well-characterized fullerene-$(R_f)_n$ derivatives, including C_1-$C_{60}(CF_3)_{2,4,6}$,[20,21] several isomers of C_1-$C_{60}(CF_3)_8$[28] and C_1-$C_{60}(CF_3)_{10}$,[25,29] C_2-$C_{60}(CF_3)_{10}$,[30] S_6-$C_{60}(CF_3)_{12}$,[31] C_1-$C_{60}(C_2F_5)_6$ and C_1-$C_{60}(C_2F_5)_8$,[32] C_1-$C_{70}(CF_3)_{2,4}$,[33] C_2-$C_{70}(CF_3)_6$,[33] the C_s and C_2 isomers of $C_{70}(CF_3)_8$,[33,34] C_1-$C_{70}(CF_3)_{10}$,[33,35] two isomers of C_1-$C_{70}(CF_3)_{12}$,[36,37] four isomers of $C_{70}(CF_3)_{14}$,[38] and two isomers of Y@$C_{82}(CF_3)_5$,[39] have their R_f substituents arranged on isolated *p*-$C_6(R_f)_2$ hexagons and/or on ribbons or loops of edge-sharing *m*- and/or *p*-$C_6(R_f)_2$ hexagons. Finally, an interesting variation of the SPP pattern has been observed for several C_s-$C_{60}X_4O$ epoxide derivatives, in which the epoxide O atom is attached to C1 and C9 and therefore assumes the role of two *ortho* σ-bonded substituents (X = NR_2[40] and *t*-BuOO[41]).

We have been studying perfluoroalkylfullerenes (PFAFs) prepared at temperatures above 400 °C because (i) they represent the only class of exohedral fullerene derivatives that do not decompose rapidly above 500 °C (with the exception of a few fluorofullerenes[42]), (ii) many of them exhibit unprecedented addition patterns,[25,29,30,32,33,35−37,39] (iii) they may include thermodynamically stable isomers of a given PFAF composition, not only kinetically stable isomers,[20,21,25,30,33,35,39] and, most importantly, (iv) they exhibit desirable physical properties that may make them suitable for the fabrication of optoelectronic devices.[43] We now report that the high-temperature reaction of C_{60} with either CF_3I or C_2F_5I in the presence of an adventitious oxygen-containing species produces, among other products, two

(16) Bergosh, R. G.; Meier, M. S.; Laske Cooke, J. A.; Spielmann, H. P.; Weedon, B. R. *J. Org. Chem.* **1997**, *62*, 7667−7672.
(17) Boltalina, O. V.; Darwish, A. D.; Street, J. M.; Taylor, R.; Wei, X.-W. *Perkin Trans. 2* **2002**, 251−256.
(18) Canteenwala, T.; Padmawar, P. A.; Chiang, L. Y. *J. Am. Chem. Soc.* **2005**, *127*, 26−27.
(19) Schulte, K.; Woolley, R. A. J.; Wang, L.; Moriarity, P. J.; Birkett, P. R.; Kroto, H. W.; Cowie, B. C. C. *Nucl. Instrum. Methods Phys. Res. A* **2005**, *547*, 208−215.
(20) Goryunkov, A. A.; Kuvychko, I. V.; Ioffe, I. N.; Dick, D. L.; Sidorov, L. N.; Strauss, S. H.; Boltalina, O. V. *J. Fluorine Chem.* **2003**, *124*, 61−64.
(21) Goryunkov, A. A.; Ioffe, I. N.; Kuvychko, I. V.; Yankova, T. S.; Markov, V. Y.; Streletskii, A. V.; Dick, D. L.; Sidorov, L. N.; Boltalina, O. V.; Strauss, S. H. *Fullerenes, Nanotubes, Carbon Nanostruct.* **2004**, *12*, 181−185.
(22) Xiao, Z.; Wang, F. D.; Huang, S. H.; Gan, L. B.; Zhou, J.; Yuan, G.; Lu, M. J.; Pan, J. Q. *J. Org. Chem.* **2005**, *70*, 2060−2066.
(23) Troyanov, S.; I.; Popov, A. A. *Angew. Chem., Int. Ed.* **2005**, *44*, 4215−4218.
(24) Avdoshenko, S. M.; Goryunkov, A. A.; Ioffe, I. N.; Ignat'eva, D. V.; Sidorov, L. N.; Pattison, P.; Kemnitz, E.; Troyanov, S., I. *Chem. Commun.* **2006**, 2463−2465.
(25) Kareev, I. E.; Kuvychko, I. V.; Lebedkin, S. F.; Miller, S. M.; Anderson, O. P.; Seppelt, K.; Strauss, S. H.; Boltalina, O. V. *J. Am. Chem. Soc.* **2005**, *127*, 8362−8375.
(26) Charton, M. *J. Am. Chem. Soc.* **1969**, *91*, 615−618.
(27) Bott, G.; Field, L. D.; Sternhell, S. *J. Am. Chem. Soc.* **1980**, *102*, 5618−5626.
(28) Kareev, I. E.; Shustova, N. B.; Newell, B. S.; Miller, S. M.; Anderson, O. P.; Strauss, S. H.; Boltalina, O. V. *J. Acta Cryst.* **2006**, *E62*, o3154−o3156.
(29) Kareev, I. E.; Lebedkin, S. F.; Miller, S. M.; Anderson, O. P.; Strauss, S. H.; Boltalina, O. V. *Acta Crystallogr.* **2006**, *E62*, o1498−o1500.
(30) Kareev, I. E.; Lebedkin, S. F.; Popov, A. A.; Miller, S. M.; Anderson, O. P.; Strauss, S. H.; Boltalina, O. V. *Acta Crystallogr.* **2006**, *E62*, o1501−o1503.
(31) Troyanov, S. I.; Dimitrov, A.; Kemnitz, E. *Angew. Chem., Int. Ed.* **2006**, *45*, 1971−1974.
(32) Kareev, I. E.; Kuvychko, I. V.; Lebedkin, S. F.; Miller, S. M.; Anderson, O. P.; Strauss, S. H.; Boltalina, O. V. *Chem. Commun.* **2006**, 308−310.
(33) Dorozhkin, E. I.; Ignat'eva, D. V.; Tamm, N. B.; Goryunkov, A. A.; Khavrel, P. A.; Ioffe, I. N.; Popov, A. A.; Kuvychko, I. V.; Streletskiy, A. V.; Markov, V. Y.; Spandl, J.; Strauss, S. H.; Boltalina, O. V. *Chem. Eur. J.* **2006**, *12*, 3876−3889.
(34) Goryunkov, A. A.; Dorozhkin, E. I.; Ignat'eva, D. V.; Sidorov, L. N.; Kemnitz, E.; Sheldrick, G. M.; Troyanov, S. I. *Mendeleev Commun.* **2005**, 225−227.
(35) Kareev, I. E.; Kuvychko, I. V.; Popov, A. A.; Lebedkin, S. F.; Miller, S. M.; Anderson, O. P.; Strauss, S. H.; Boltalina, O. V. *Angew. Chem., Int. Ed.* **2005**, *44*, 7984−7987.
(36) Kareev, I. E.; Lebedkin, S. F.; Miller, S. M.; Anderson, O. P.; Strauss, S. H.; Boltalina, O. V. *Acta Crystallogr.* **2006**, *E62*, o620−o622.
(37) Kareev, I. E.; Lebedkin, S. F.; Miller, S. M.; Anderson, O. P.; Strauss, S. H.; Boltalina, O. V. *Acta Crystallogr.* **2006**, *E62*, o617−o619.
(38) Goryunkov, A. A.; Ignat'eva, D. V.; Tamm, N. B.; Moiseeva, N. N.; Ioffe, I. N.; Avdoshenko, S. M.; Markov, V. Y.; Sidorov, L. N.; Kemnitz, E.; Troyanov, S. I. *Eur. J. Org. Chem.* **2006**, 2508−2512.
(39) Kareev, I. E.; Lebedkin, S. F.; Bubnov, V. P.; Yagubskii, E. B.; Ioffe, I. N.; Khavrel, P. A.; Kuvychko, I. V.; Strauss, S. H.; Boltalina, O. V. *Angew. Chem., Int. Ed.* **2005**, *44*, 1846−1849.
(40) Isobe, H.; Ohbayashi, A.; Sawamura, M.; Nakamura, E. *J. Am. Chem. Soc.* **2000**, *122*, 2669−2670.
(41) Gan, L. B.; Huang, S. H.; Zhang, X. A.; Zhang, A. X.; Cheng, B. C.; Cheng, H.; Li, X. L.; Shang, G. *J. Am. Chem. Soc.* **2002**, *124*, 13384−13385.
(42) Boltalina, O. V.; Strauss, S. H. In *Dekker Encyclopedia of Nanoscience and Nanotechnology*; Schwarz, J. A., Contescu, C., Putyera, K., Eds.; Marcel Dekker: New York, 2004; pp 1175−1190.
(43) Popov, A. A.; Tarabek, J.; Kareev, I. E.; Lebedkin, S. F.; Strauss, S. H.; Boltalina, O. V.; Dunsch, L. *J. Phys. Chem. A* **2005**, *109*, 9709−9711.

PFAF epoxides with the SPP addition pattern, 6,12,15,18-tetrakis(trifluoromethyl)-6,12,15,18-tetrahydrooxireno-[2′,3′:1,9]-(C_{60}-I_h)[5,6]fullerene (C_s-$C_{60}(CF_3)_4O$) and 6,12,15,18-tetrakis-(pentafluoroethyl)-6,12,15,18-tetrahydrooxireno-[2′,3′:1,9](C_{60}-I_h)[5,6]fullerene (C_s-$C_{60}(C_2F_5)_4O$). These are the first well-characterized PFAFs that also contain non-fluorine-containing exohedral substituents, opening up possibilities for the conversion of PFAFs into covalently linked molecular assemblies. In addition, they are also the first fullerene epoxides known to be stable at temperatures exceeding 400 °C. In addition, we have isolated and characterized the compound 1,6,9,12,15,18-hexakis-(trifluoromethyl)-1,6,9,12,15,18-hexahydro(C_{60}-I_h)[5,6]fullerene (C_s-$C_{60}(CF_3)_6$), demonstrating that the SPP pattern can be formed above 500 °C for fullerene$(R_f)_n$ derivatives with fewer than 16 substituents.

Experimental Section

Reagents and Solvents. HPLC-grade toluene, hexane, heptane (Fisher), C_{60} (99.9+ Super Gold Grade, Hoechst), *m*-xylene, 40-mesh copper powder (99.5%), CF_3I (99+%), C_2F_5I (97%), and sulfur (S_8) (Sigma Aldrich) were used as received. Hexafluorobenzene (Sigma Aldrich) and toluene-d_8 (Cambridge Isotopes) were dried over an appropriate drying agent and vacuum-distilled. The compounds C_s-$C_{60}Cl_6$[6] and C_1-$C_{60}(CF_3)_6$[20] were prepared by literature methods.

Preparation and Isolation of C_s-$C_{60}(C_2F_5)_4O$. In a typical synthesis, a finely ground sample of C_{60} (90 mg, 0.13 mmol) was mixed with 40-mesh copper powder (500 mg, 7.87 mmol) and heated in a glass tube to 430 °C under an argon atmosphere, as previously described.[25,32] Gaseous C_2F_5I was passed through the heated tube during 2−4 h. [***Caution***: C_2F_5I decomposes above 300 °C in air and can produce toxic HF, COF_2, and I_2; handle only in a well-ventilated fume hood.] Dark-brown PFAF derivatives and purple I_2 condensed inside the tube approximately 1 cm outside of the downstream end of the furnace (i.e., in the downstream cold zone). Iodine was removed under a flow of argon with mild heating (ca. 100 °C), and the dark-brown condensate was dissolved in toluene and processed by HPLC (20 mm i.d. × 250 mm long Cosmosil Buckyprep column (Nacalai Tesque, Inc.), 300 nm UV detector, toluene or 40:60 (v:v) toluene:hexane eluent, 18 mL min^{-1} flow rate).

Toluene was the HPLC eluent for the first stage of purification, and among other $C_{60}(C_2F_5)_{4-10}$ compounds (two of which have already been reported[32] and the rest of which will be described in a separate paper) was a fraction that eluted between 5.0 and 7.3 min. This fraction was purified in a second stage of purification by eluting again with toluene, and a fraction that eluted between 5.8 and 6.1 min was collected. The final stages of purification, which were repeated three times, involved elution with 40:60 (v:v) toluene:hexane, and a red-orange fraction that eluted between 20.4 and 23.1 min was collected, as shown in the bottom panel in Figure S-2 (Supporting Information). Slow evaporation of the solvent led to the isolation of several milligrams of red-orange crystals. According to MS and NMR analyses, the purity of samples of C_s-C_{60}-$(C_2F_5)_4O$ prepared and purified by this procedure was greater than 97%.

Preparation and Isolation of C_s-$C_{60}(CF_3)_4O$ and C_s-$C_{60}(CF_3)_6$. Reactions between C_{60} and a stream of heated CF_3I at 460, 550, or 600 °C proceeded in a fashion similar to that described above, except that copper powder was not used. [***Caution***: CF_3I decomposes above 300 °C in air and can produce toxic HF, COF_2, and I_2; handle only in a well-ventilated fume hood.] In each case, the dark-brown cold-zone condensate was dissolved in toluene and processed by HPLC in a manner similar to that described above. Subsequent HPLC processing of the 550 °C reaction products is shown in Figures 2 and S-2. Workup of products from several 550 °C reactions led to the isolation of ca. 20 mg of red-orange crystalline C_s-$C_{60}(CF_3)_4O$ and several milligrams of C_s-$C_{60}(CF_3)_6$, both of which appeared to be 97+% pure by MS and NMR analysis. HPLC chromatograms for the crude mixtures of products for the three reaction temperatures are shown in Figure 3.

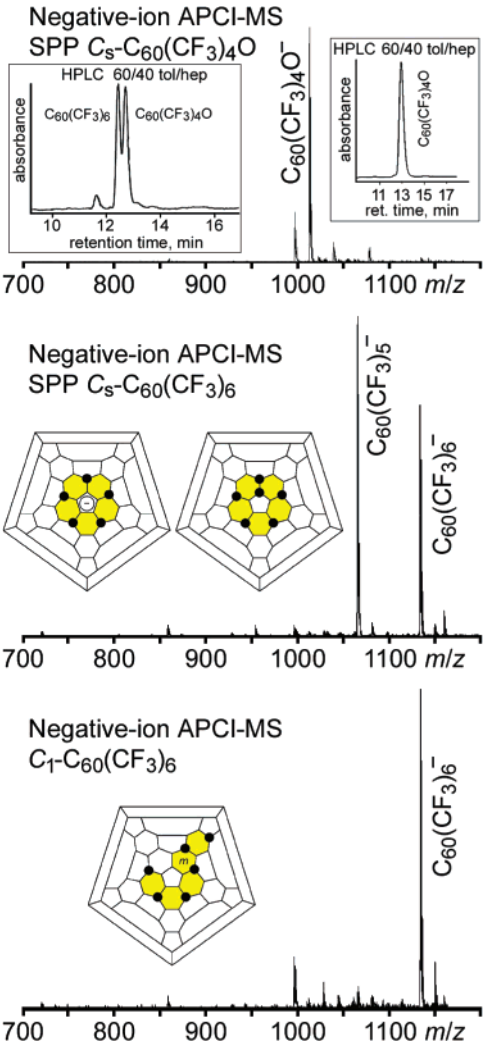

Figure 2. (Top) Negative-ion APCI mass spectrum and HPLC trace of purified C_s-$C_{60}(CF_3)_4O$. The left inset shows the HPLC trace before purification, which indicates nearly equal amounts of C_s-$C_{60}(CF_3)_4O$ and C_s-$C_{60}(CF_3)_6$. (Middle) Negative-ion APCI mass spectra of purified C_s-$C_{60}(CF_3)_6$, also showing the Schlegel diagram for the stable cyclopentadienide structure $C_{60}X_5^-$. (Bottom) Negative-ion APCI mass spectrum of C_1-$C_{60}(CF_3)_6$. All spectra were recorded under identical conditions and using identical instrument parameters.

Spectroscopic Characterization. Matrix-assisted laser desorption/ionization (MALDI) time-of-flight mass spectra were recorded using a Voyager-DE PRO Workstation (Applied Biosystems). Sulfur was used as the matrix material. It was mixed with the sample in toluene or toluene/hexane immediately prior to deposition on the target. Nitrogen laser pulses of 337 nm wavelength, 0.5 ns duration, and 3 Hz frequency were used to desorb the species into the gas phase. The negative or positive ions formed were detected in reflectron mode. Atmospheric-pressure chemical ionization (APCI) mass spectra were recorded on a Finnigan (ThermoQuest) LCQ DUO mass spectrometer (hexane or acetonitrile eluent, 0.3 mL min^{-1} flow rate). Samples for ^{19}F NMR spectroscopy were benzene-d_6 solutions containing a small amount of hexafluorobenzene as an internal standard (δ −164.9). Spectra were recorded using a Varian INOVA-unity 400 spectrometer operating at 367.45 MHz. FT-Raman measurements were performed on powdered samples at room temperature using a Bruker Equinox 55S spectrometer equipped with a FRA106 FT-Raman module and a continuous-wave Nd:YAG laser for excitation at 1064 nm. The typical laser power

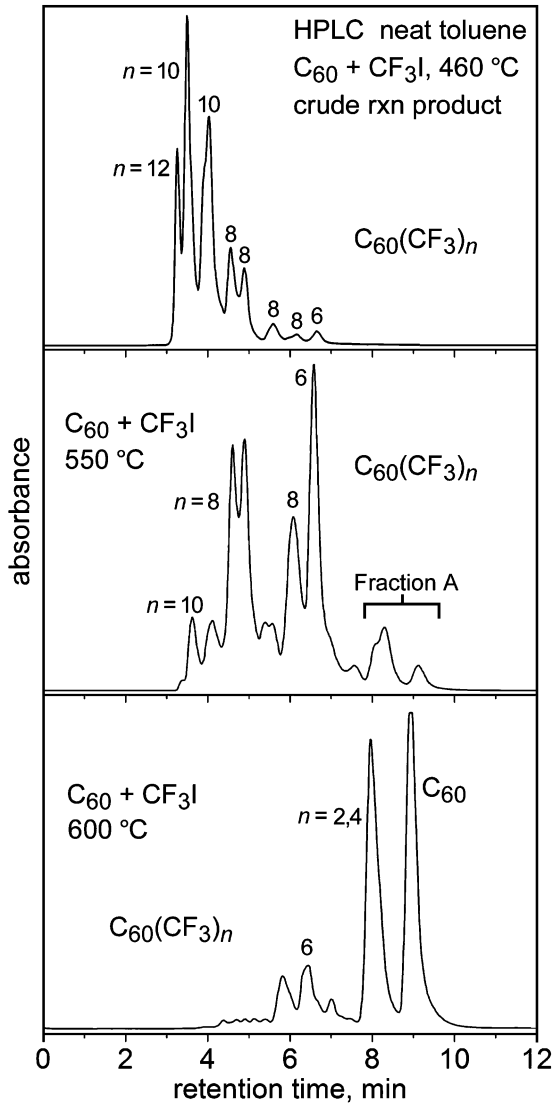

Figure 3. HPLC chromatograms of the crude, cold-zone condensed products of the reactions of C_{60} with CF_3I at 460, 550, and 600 °C. See Figure S-2 for the workup of Fraction A.

(excitation intensity) and spectral resolution used were 50 mW (ca. 10^3 W cm^{-2}) and 4 cm^{-1}, respectively. Relatively long acquisition times (ca. 2−3 h) were necessary to increase the signal-to-noise ratio. The spectra had a broad, moderately intense luminescence background, which was digitally subtracted. An important advantage of near-infrared (NIR) excitation is that the luminescence background would have been much stronger with visible-wavelength excitation. Another important advantage is the reduced tendency for samples to undergo photochemical reactions (such as laser photoinduced polymerization, which has been observed for C_{60}[44]). Electronic spectra were recorded using a Varian Cary 500 UV−Vis−NIR spectrophotometer.

X-ray Crystallography. X-ray diffraction data from crystals of C_s-$C_{60}(CF_3)_4O$·*m*-xylene and C_s-$C_{60}(C_2F_5)_4O$ (grown by slow evaporation from saturated *m*-xylene or toluene solutions, respectively) were recorded on a Bruker Kappa APEX II CCD diffractometer employing Mo Kα radiation (graphite monochromator). Selected details related to the crystallographic experiments are listed in Table 1. Unit cell parameters were obtained from least-squares fits to the angular coordinates of all reflections, and intensities were integrated from a series of frames (ω and ϕ rotation) covering more than a hemisphere of reciprocal space. Absorption and other corrections were applied by using SADABS.[45] The structures were solved by using direct methods and refined (on F^2, using all data) by a full-matrix, weighted least-squares process. All atoms were refined by using anisotropic atomic displacement parameters, with the exception of two of the C atoms of the disordered *m*-xylene molecule in $C_{60}(CF_3)_4O$·*m*-xylene. Given the unusual values of the atomic displacement parameters associated with the carbon atoms in the disordered solvent molecule, it was considered inappropriate to add hydrogen atoms to these atoms. Standard Bruker control and integration software (APEX II) was employed, and Bruker SHELXTL[46] software was used for structure solution, refinement, and graphics.

Table 1. Crystal Data and Structure Refinement for C_s-$C_{60}(C_2F_5)_4O$ and C_s-$C_{60}(CF_3)_4O$·*m*-$C_6H_4(CH_3)_2$

	C_s-$C_{60}(C_2F_5)_4O$	C_s-$C_{60}(CF_3)_4O$·*m*-$C_6H_4(CH_3)_2$
molecular formula	$C_{68}F_{20}O$	$C_{68}H_8F_{12}O$
formula weight	1212.68	1065.72
crystal system	triclinic	monoclinic
space group	$P\bar{1}$	$C2/c$
Z	2	8
color of crystal	red-orange	red-orange
unit cell dimensions		
a, Å	10.1145(6)	40.2225(8)
b, Å	12.3096(8)	10.1706(3)
c, Å	18.8423(8)	20.1770(4)
α, °	80.148(3)	90
β, °	78.049(3)	114.193(1)
γ, °	74.893(3)	90
temperature, K	100(1)	100(1)
final R indices	$R_1 = 0.0536$	$R_1 = 0.0495$
$[I > 2\sigma(I)]$	$wR_2 = 0.1093$	$wR_2 = 0.1133$
goodness-of-fit on F^2	0.959	1.008

Quantum Chemical Calculations. Molecular structures and harmonic vibrational frequencies were calculated at the DFT level of theory with the PRIRODA package[47] using the GGA functional of Perdew, Burke, and Ernzerhof (PBE).[48] The TZ2P-quality Gaussian basis set {6,1,1,1,1,1/4,1,1/1,1} was used for carbon and fluorine atoms. The quantum-chemical code employed expansion of the electron density in an auxiliary basis set to accelerate the evaluation of the Coulomb and exchange-correlation terms. Raman intensities were computed numerically at the PBE/6-31G level using the PC version[49] of the GAMESS quantum-chemical package. AM1 calculations were also performed with the PC version of GAMESS.

Results

High-Temperature Reactions of C_{60} with CF_3I and C_2F_5I. The addition of CF_3 or C_2F_5 groups to C_{60} with a stream of CF_3I or C_2F_5I in a hot tube is thought to involve the sequential addition of thermally generated CF_3 or C_2F_5 radicals to solid C_{60} until the volatilities of the $C_{60}(R_f)_n$ products are high enough for them to sublime out of the hot reaction zone.[25,32] Therefore, the distribution of products is strongly dependent on the reaction temperature, the length of the hot zone, the temperature gradient, and the R_fI flow rate. Figure 3 shows the effect of changing just one variable, the reaction temperature, from 460 to 550 to 600 °C for a series of C_{60}/CF_3I reactions. Compounds with higher n values are more volatile than those with lower n values,[25,32,33,35] and for this reason PFAFs with the lowest n

(44) Dresselhaus, M. S.; Dresselhaus, G.; Eklund, P. C. *J. Raman Spectrosc.* **1996**, *27*, 351−371.
(45) Sheldrick, G. M. *SADABS—A program for area detector absorption corrections*; Bruker AXS: Madison, WI, 1996.
(46) Sheldrick, G. M. *SHELXTL*, v. 6.14; Bruker AXS: Madison, WI, 2004.
(47) Laikov, D. N. *Chem. Phys. Lett.* **1997**, *281*, 151−156.
(48) Perdew, J. P.; Burke, K.; Ernzerhof, M. *Phys. Rev. Lett.* **1996**, *77*, 3865−3868.
(49) Granovsky, A. A. *PC GAMESS*, v. 7.0 (http://classic.chem.msu.su/gran/gamess/index.html).

values (2, 4, 6) were most abundant at the highest reaction temperature. However, the 600 °C product mixture also contained a significant amount of sublimed C_{60}, so the conversion of C_{60} to PFAFs with $n = 2$, 4, and 6 was actually higher at 550 °C than at 600 °C. Two compounds isolated with high purity for the first time, C_s-$C_{60}(CF_3)_4O$ and C_s-$C_{60}(CF_3)_6$, were discovered in HPLC Fraction A (see Figure 3), and they, along with a third new compound, C_s-$C_{60}(C_2F_5)_4O$, are the subject of this paper. We are continuing to optimize experimental conditions so that high yields of narrow ranges of PFAF compositions may be prepared, and when completed those studies will be published elsewhere.

Further HPLC processing of C_{60}/CF_3I fraction A led to the isolation of three main fractions, as shown in Figure S-2. An S_8-MALDI mass spectrum of fraction A3 (see inset in the middle panel in Figure S-2) showed that it contained predominantly $C_{60}(CF_3)_4O$ plus small amounts of C_{60} and an isomer of $C_{60}(CF_3)_6$ with a retention time significantly different than that of the C_1-p^3mp-$C_{60}(CF_3)_6$ isomer reported by us in 2003.[20] When the microcrystalline solid obtained by evaporating the solvents from fraction A3 was extracted with neat heptane, an approximately equimolar solution of C_s-$C_{60}(CF_3)_4O$ and C_s-$C_{60}(CF_3)_6$ was obtained. These compounds were separated by HPLC, as shown in Figure 2, and the solid that remained after the heptane extraction was shown by MS and NMR analysis to be 97+% pure C_s-$C_{60}(CF_3)_4O$.

The compound C_s-$C_{60}(C_2F_5)_4O$ represents a minor fraction of all $C_{60}(C_2F_5)_n$ derivatives prepared by treating C_{60} with C_2F_5I in a hot tube, two of which, C_1-p,p,p-$C_{60}(C_2F_5)_6$ and C_1-p^3mp,p-$C_{60}(C_2F_5)_8$, have already been described.[32] It was isolated in milligram amounts, as shown in the bottom panel in Figure S-2. The S_8-MALDI mass spectrum (inset in the bottom panel in Figure S-2) and NMR spectrum (see below) indicated that its compositional and isomeric purity was at least 97%.

X-ray Structures of C_s-$C_{60}(C_2F_5)_4O$ and C_s-$C_{60}(CF_3)_4O$. The molecular structures of C_s-$C_{60}(C_2F_5)_4O$ and C_s-$C_{60}(CF_3)_4O$ are shown in Figures 4 and S-3 (Supporting Information). The complete carbon atom numbering scheme for both molecules, which is the IUPAC-recommended numbering scheme,[50] is shown in Figure S-4 in the Supporting Information. Selected interatomic distances and angles are listed in Table 2, which also lists these parameters for the DFT-optimized structures and for several related compounds.

The perfluoroethyl derivative crystallized without the inclusion of solvent molecules. The epoxide O atom is attached to C1 and C9. Bond distances and angles within the C_2O oxirane ring are similar to those in other structurally characterized [60]-fullerene epoxide derivatives.[7,51,52] The four C_2F_5 groups are attached to C6, C12, C15, and C18, forming a ribbon of three edge-sharing p-$C_6(C_2F_5)_2$ hexagons (each shared edge is a $C(sp^2)-C(sp^3)$ bond). The conformation of each C_2F_5 group is staggered with respect to the three cage C−C bonds radiating from the C atom to which it is attached, as shown in Figure S-5 (Supporting Information) for the C_2F_5 group attached to C6. This orients the CF_2 F atoms of the C15 and C18 C_2F_5 groups over their respective shared p-$C_6(C_2F_5)_2$ hexagons, resulting in three F···F contacts that range from 2.469(5) to 2.578(5) Å.

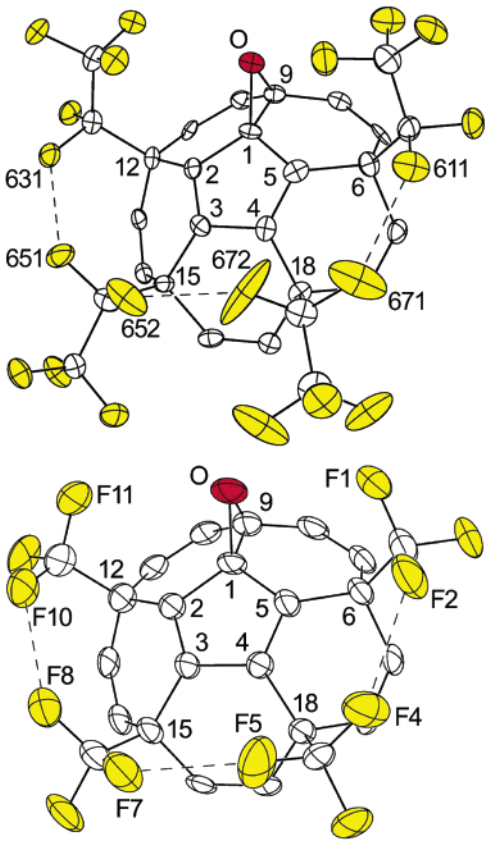

Figure 4. (Top) Drawing of the X-ray structure of C_s-$C_{60}(C_2F_5)_4O$, showing only the portion of the molecule bearing the five substituents (50% probability ellipsoids; one- and two-digit numbers are carbon atom numbers; three-digit numbers are fluorine atom numbers). Fluorine atoms are highlighted. Selected interatomic distances (Å) and angles (deg): C1−C9, 1.511(7); C1−O, 1.450(6); C9−O, 1.432(6); C1−O−C9, 63.2(3); C1−C9−O, 58.9(3); C9−C1−O, 57.8(3); C1−C2, 1.481(7); C1−C5, 1.476(7); C2−C3, 1.358(7); C3−C4, 1.496(7); C4−C5, 1.361(7); tors C2−C3−C4−C5, 1.0; F631···F651, 2.521(6); F652···F672, 2.578(6); F611···F671, 2.469(6). (Bottom) Drawing of the X-ray structure of C_s-$C_{60}(CF_3)_4O$, showing only the portion of the molecule bearing the five substituents (50% probability ellipsoids; one- and two-digit numbers are carbon atom numbers). Fluorine atoms are highlighted. Selected interatomic distances (Å) and angles (deg): C1−C9, 1.488(6); C1−O, 1.447(5); C9−O, 1.413(6); C1−O−C9, 62.7(3); C1−C9−O, 59.8(3); C9−C1−O, 57.5(2); C1−C2, 1.482(5); C1−C5, 1.481(5); C2−C3, 1.342(5); C3−C4, 1.480(5); C4−C5, 1.353(5); tors C2−C3−C4−C5, 0.5; F2···F4, 2.582(5); F5···F7, 2.550(5); F8···F10, 2.634(5).

The molecules of C_s-$C_{60}(C_2F_5)_4O$ are packed so that there are chains of neighboring molecules that are connected via $\pi-\pi$ intermolecular contacts between coplanar hexagons, as shown in Figure S-6 in the Supporting Information (the interplanar spacings are 3.40 and 3.44 Å). The closest contacts between the chains are C56···C56′ interactions of 2.92 Å. There are also (presumably weaker) intermolecular interactions between the fluorous portions of other nearest neighbors, with 12 intermolecular F···F contacts between a pair of nearest neighbors ranging from 2.77 to 3.18 Å, as also shown in Figure S-6.

The trifluoromethyl derivative crystallized with a disordered molecule of m-xylene in the asymmetric unit. The four CF_3 groups are also staggered (see Figure S-5), and the three closest F···F contacts between the four CF_3 groups range from 2.550(5)

(50) Powell, W. H.; Cozzi, F.; Moss, G. P.; Thilgen, C.; Hwu, R. J. R.; Yerin, A. *Pure Appl. Chem.* **2002**, *74*, 629−695.
(51) Balch, A. L.; Costa, D. A.; Lee, J. W.; Noll, B. C.; Olmstead, M. M. *Inorg. Chem.* **1994**, *33*, 2071−2072.
(52) Al-Matar, H.; Hitchcock, P. B.; Avent, A. G.; Taylor, R. *Chem. Commun.* **2000**, 1071−1072.

Table 2. Selected Interatomic Distances (Å) and Angles (deg)[a]

	C_s-$C_{60}(C_2F_5)_4O$		C_s-$C_{60}(CF_3)_4O$		C_s-$C_{60}Br_6$		C_s-$C_{60}(CF_3)_6$	C_s-$C_{60}(CH_3)_6$	C_s-$C_{60}(NR_2)_4O$	$C_{60}(CF_3)_{10}$-4	*cis*-C_4H_6
	X-ray	DFT	X-ray	DFT	X-ray[b]	DFT	DFT	X-ray[c]	X-ray[d]	X-ray[e]	MP2[f]
C1−C9	1.511(7)	1.511	1.488(6)	1.512	1.557(4)	1.565	1.603	1.540(9)	1.49(3)	1.508(3)	
C1−O	1.450(6)	1.442	1.447(6)	1.443							
C9−O	1.432(6)	1.419	1.413(6)	1.419							
C1−O−C9	63.2(3)	63.8	62.7(3)	63.8							
C1−C9−O	58.9(3)	58.8	59.8(3)	58.9							
C9−C1−O	57.8(3)	57.4	57.5(2)	57.3							
C1−*C2*	1.481(7)	1.491	1.482(5)	1.490			1.550				
C1−C5	1.476(7)	1.492	1.481(5)	1.490			1.551				
C2−C3	1.358(7)	1.364	1.342(5)	1.364	1.350(4)	1.362	1.358	1.349(9)	1.29(3)	1.347(3)	1.343
C3−C4	1.496(7)	1.484	1.480(5)	1.487	1.462(4)	1.463	1.479	1.460(9)	1.51(3)	1.481(3)	1.470
C4−C5	1.361(7)	1.365	1.353(5)	1.364	1.349(4)	1.362	1.358	1.364(9)	1.35(3)	1.344(3)	1.343
F···F	2.521(6)[g]	2.732[g]	2.582(5)[j]	2.646[j]			2.683[j]				
F···F	2.578(6)[h]	2.672[h]	2.550(5)[k]	2.597[k]			2.584[k]				
F···F	2.469(6)[i]	2.554[i]	2.634(5)[l]	2.646[l]			2.654[l]				

[a] All data from this work unless otherwise noted. [b] Reference 4. [c] Reference 7. [d] Reference 40. [e] Reference 30; $C_{60}(CF_3)_{10}$-4 = 1,6,12,15,18,25,41,45,57-$C_{60}(CF_3)_{10}$. [f] Reference 53. [g] F631···F651. [h] F652···F672. [i] F611···F671. [j] F2···F4. [k] F5···F7. [l] F8···F10.

to 2.634(5) Å. The structure of the fullerene cage in C_s-C_{60}-$(CF_3)_4O$ is virtually identical to the C_2F_5 homologue (see Table 2). However, the solid-state packing in C_s-$C_{60}(CF_3)_4O$·*m*-xylene is different than the packing in C_s-$C_{60}(C_2F_5)_4O$ in a significant way. The C_s-$C_{60}(CF_3)_4O$ molecules are aligned *head-to-tail* in rows (unlike the head-to-head alignment between rows in C_s-$C_{60}(C_2F_5)_4O$). The interplane separation between the C1−C5 and C56′−C60′ pentagons in neighboring molecules in a given row is 3.49 Å, as shown in Figure S-7 (Supporting Information), and the least-squares planes of these two pentagons are tilted only 3.3° from one another. The head-to-tail rows in C_s-C_{60}-$(CF_3)_4O$·*m*-xylene are packed in layers. A portion of one layer is shown in Figure S-7 (the four molecules shown lie in the plane of the page). In addition, the layers are held together by $\pi-\pi$ intermolecular contacts between the {C28−C31,C47−C48} and {C19−C21,C38−C40} hexagons on neighboring molecules that are tilted 14.3° from one another. The distance between the centroids of these neighboring hexagons is 3.63 Å. There are only two intermolecular F···F contacts shorter than 3.0 Å (F5···F7′, 2.891 Å; F4···F12′, 2.913 Å).

Spectroscopic Characterization. (a) Fluorine-19 NMR Spectroscopy. Room-temperature spectra for the two new epoxides are shown in Figure 5. In both cases, the spectra indicate that the samples were at least 97% pure. The spectrum of C_s-$C_{60}(CF_3)_4O$ consists of equal-intensity mutually coupled multiplets at δ −67.7 and −68.1, a pattern that is consistent with the idealized C_s-symmetry X-ray structure. The small $\Delta\delta$ value has rendered the expected quartets into more complex second-order-coupled multiplets, but an approximate $^7J_{FF}$ value of 12 Hz is apparent. In 2003, we assigned an impurity that exhibited two multiplets with the same δ values in a sample of 1,7-$C_{60}(CF_3)_2$ to the then-unknown isomer C_s-p^3-$C_{60}(CF_3)_4$.[20] We now believe it is more likely that the impurity was C_s-C_{60}-$(CF_3)_4O$, although it is possible that the putative compound C_s-p^3-$C_{60}(CF_3)_4$ would exhibit a nearly identical spectrum. However, it is probably the case that C_s-p^3-$C_{60}(CF_3)_4$ was not the impurity observed in our sample of 1,7-$C_{60}(CF_3)_2$ and that C_1-*pmp*-$C_{60}(CF_3)_4$ is still the only isomer of $C_{60}(CF_3)_4$ that has been isolated as a pure compound and unambiguously characterized.

The ^{19}F NMR spectrum of C_s-$C_{60}(C_2F_5)_4O$ consists of two sharp, equal-intensity singlets in the CF_3 region at δ −80.2 and −80.8 and a complex pattern of multiplets in the CF_2 region

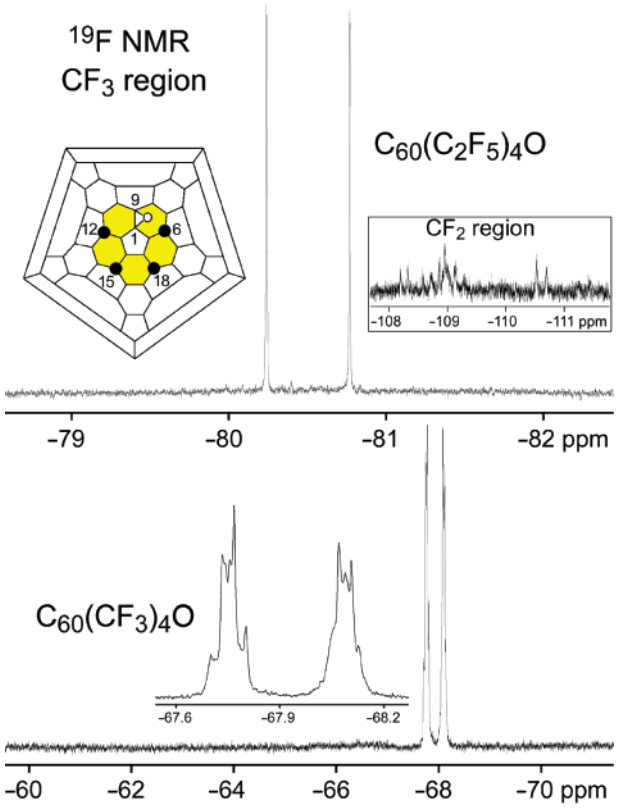

Figure 5. Fluorine-19 NMR spectra of C_s-$C_{60}(C_2F_5)_4O$ and C_s-$C_{60}(CF_3)_4O$ (376.5 MHz; 20 °C; toluene-d_8; C_6F_6 internal standard, δ −164.9).

that extends from δ −108 to −112. The lack of observable $^3J_{FF}$ coupling between the F atoms in the CF_2 and CF_3 moieties of a given C_2F_5 group is not uncommon.[54,55] Furthermore, no such coupling was observed in the ^{19}F NMR spectra of C_1-*p,p,p*-$C_{60}(C_2F_5)_6$ and C_1-p^3*mp,p*-$C_{60}(C_2F_5)_8$.[32] The CF_2 multiplets of those two compounds were also very complex and have not yet been unambiguously assigned to specific F atoms in the CF_2 groups.

(53) De Mare, G. R.; Panchenko, Y. N.; Vander Auwera, J. *J. Phys. Chem. A* **1997**, *101*, 3998−4004.
(54) Emsley, J. W.; Phillips, L.; Wray, V. *Fluorine Coupling Constants*; Pergamon: Oxford, UK, 1977.
(55) Stern, G. A.; Westmore, J. B. *Can. J. Chem.* **1999**, *77*, 1734−1744 and references therein.

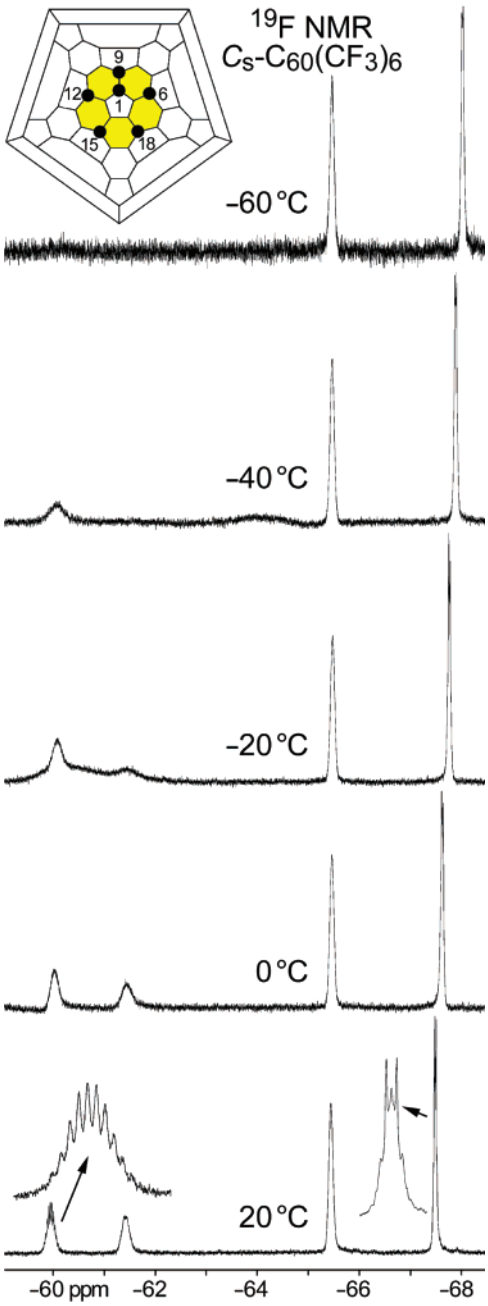

Figure 6. Variable-temperature ^{19}F NMR spectra of C_s-$C_{60}(CF_3)_6$ (376.5 MHz; toluene-d_8; C_6F_6 internal standard, δ −164.9).

Variable-temperature spectra for C_s-$C_{60}(CF_3)_6$ are shown in Figure 6. The 20 °C spectrum consists of four multiplets at δ −59.9 (intensity (int.) 1), −61.4 (int. 1), −65.4 (int. 2), and −67.5 (int. 2). The δ −59.9 multiplet is an apparent dectet with splittings of 11 Hz. The δ −67.5 multiplet is clearly second-order in nature and is assigned to the CF_3 groups on C15 and C18, which are symmetry equivalent but not magnetically equivalent. The other two multiplets are unresolved. As the temperature was lowered from 20 to −80 °C, the δ −65.4 and −67.5 multiplets are only slightly broadened (the −80 °C spectrum is not shown but was identical to the −60 °C spectrum). However, lowering the temperature broadened the other two multiplets to the point of complete decoalescence. The δ −61.4 multiplet underwent decoalescence at a higher temperature than the δ −59.9 multiplet.

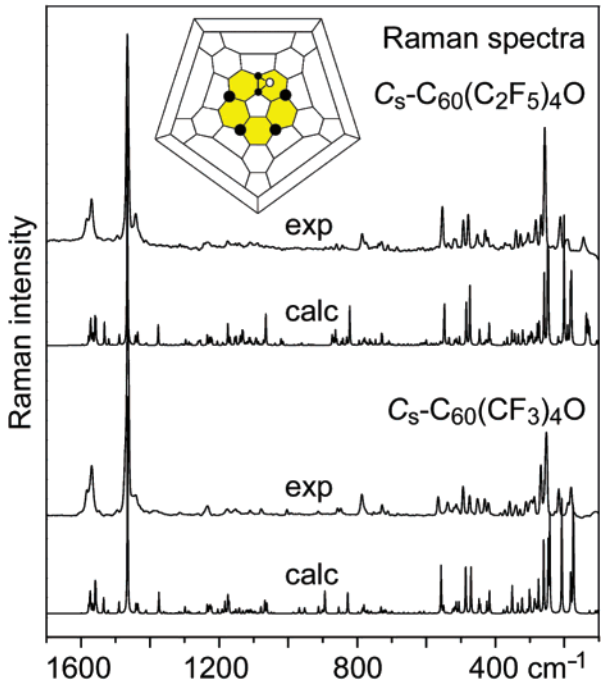

Figure 7. Experimental and DFT-calculated Raman spectra of C_s-$C_{60}(C_2F_5)_4O$ and C_s-$C_{60}(CF_3)_4O$.

(b) Raman Spectroscopy. Raman spectra of C_s-$C_{60}(C_2F_5)_4O$ and C_s-$C_{60}(CF_3)_4O$ are shown in Figure 7, along with the corresponding DFT-predicted spectra. Both compounds exhibit nearly congruent spectra, dominated by a very strong band at 1465 cm^{-1} and a group of medium- to strong-intensity bands in the 150−550 cm^{-1} range (the highest-intensity band is at 253 cm^{-1} in $C_{60}(CF_3)_4O$ and at 258 cm^{-1} in $C_{60}(C_2F_5)_4O$). The most intense bands in the 1064 nm Raman spectrum of C_{60} are observed at 273 ($H_g(1)$) and 1468 cm^{-1} ($A_g(2)$), so it appears that the band-intensity distribution in $C_{60}(R_f)_4O$ Raman spectra is inherited from C_{60}, which demonstrates that the observed bands are largely due to cage-vibration normal modes. The DFT-calculated Raman spectra are in good agreement with the experimental spectra.

(c) Electronic Spectroscopy. The electronic spectra from 300 to 620 nm of heptane solutions of C_s-$C_{60}(CF_3)_4O$, C_s-$C_{60}(CF_3)_6$, and C_s-$C_{60}Cl_6$ are shown in Figure 8. Visible absorption spectra of fullerenes and their derivatives are due mostly to $\pi^*\leftarrow\pi$ excitations and are structure sensitive.[13,56,57] Compounds with the same addition pattern usually exhibit similar spectra with similar band positions and bandwidths irrespective of the substituents (unless the substituents are also chromophores), and hence absorption spectra may be used in favorable cases for tentative structure elucidation. The designation of particular spectral features, labeled **a**−**f** in Figure 8, follows the notation in ref 13 for the SPP compounds C_s-$C_{60}Ph_5X$ (X = Cl, H, OH).

Quantum Chemical Calculations. In order to understand the trends in stability of possible $C_{60}(R_f)_4O$ isomers, we have performed series of AM1 and DFT calculations of various isomers of $C_{60}(CF_3)_4O$. When the fullerene epoxide $C_{60}O$ was originally studied, two possible structures were considered, addition of the O atom to a hex−hex junction, forming an

(56) Marchesan, S.; da Ros, T.; Prato, M. *J. Org. Chem.* **2005**, *70*, 4706−4713.
(57) Kordatos, K.; Bosi, S.; da Ros, T.; Zambon, A.; Lucchini, V.; Prato, M. *J. Org. Chem.* **2001**, *66*, 2802−2808.

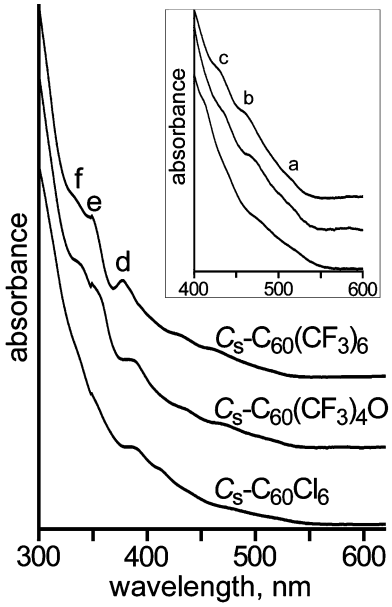

Figure 8. Electronic spectra of heptane solutions of C_s-$C_{60}(CF_3)_6$, C_s-$C_{60}(CF_3)_4O$, and C_s-$C_{60}Cl_6$. The spectra have been deliberately offset for clarity.

epoxide (the 6/6 epoxide), or insertion of the O atom into a hex−hex junction C−C bond, forming an ether (the 6/6 ether, an oxa-homofullerene). Spectroscopic data indicated that $C_{60}O$ was in fact an epoxide.[58] Raghavachari considered a third possible structure, the 5/6 ether, and found it to be 25 and 38 kJ mol^{-1} more stable than the 6/6 epoxide at the semi-empirical and HF/3-21G levels, respectively.[59] However, extensions of the basis set or the use of DFT have both shown that the 6/6 epoxide and the 5/6 ether are essentially isoenergetic, the epoxide being favored by only 2 kJ mol^{-1} at the DFT level,[60] and the 5/6 ether was subsequently isolated and characterized.[61] The fourth possible isomer, the 5/6 epoxide, was reported to convert to the 5/6 ether in the course of geometry optimization.[62]

Our DFT calculations also predict that the 6/6 epoxide isomer of $C_{60}O$ is 2.3 kJ mol^{-1} more stable than the 5/6 ether. Furthermore, the 6/6 ether did not represent a potential-energy minimum and was converted to the 6/6 epoxide during optimization. However, we have found that isomers of $C_{60}(CF_3)_4O$ can have any of the four possible oxygen-containing $C_{60}O$ moieties, resulting in 6/6 epoxides, 6/6 ethers, 5/6 epoxides, and 5/6 ethers. In order to find the most stable isomers, we considered structures having one of the four $C_{60}O$ moieties combined with two *p*-$C_6(CF_3)_2$ hexagons, in which the hexagons were either isolated from one another or combined to form p^3 or *pmp* ribbons. At the AM1 level of theory, we considered ca. 330 6/6 epoxides, ca. 330 6/6 ethers, 36 5/6 epoxides, and ca. 660 5/6 ethers. For each series, 10−30 of the lowest-energy isomers were re-optimized at the DFT level. A complete list of the relative energies of the 85 DFT structures is given in Table S-1 in the Supporting Information. Figure 9 shows the nine most stable structures, which will be discussed below.

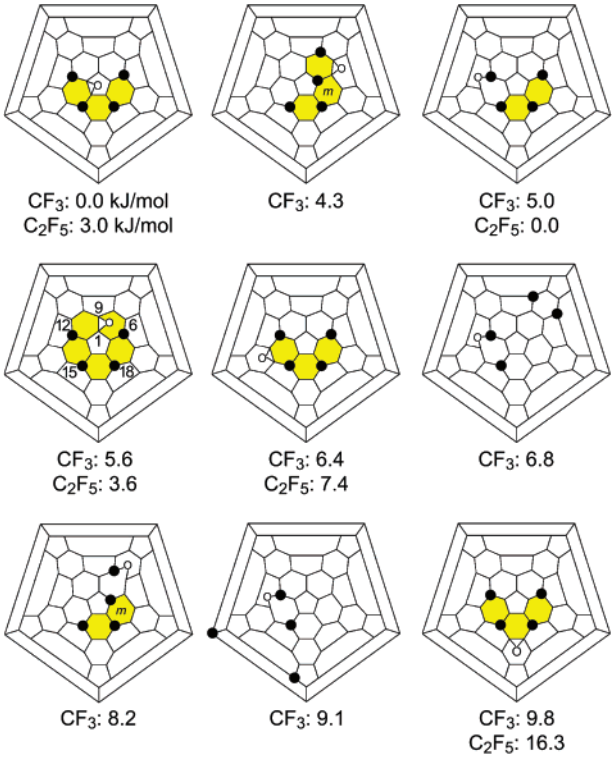

Figure 9. Schlegel diagrams of the nine most stable DFT-predicted ether (oxahomofullerene) or epoxide (oxirenofullerene) isomers of $C_{60}(CF_3)_4O$. Under each diagram is the DFT-predicted relative $\Delta H_f°$ value. Also shown are the DFT-predicted $\Delta H_f°$ values for the lowest-energy conformations of several isomers of $C_{60}(C_2F_5)_4O$. Several tris(trifluoromethyl)trifluoromethoxy derivatives are more stable than these isomers but are not included in this figure (the most stable $C_{60}(CF_3)_3(OCF_3)$ isomer has a relative $\Delta H_f°$ value of −52.0 kJ mol^{-1}).

We also performed DFT calculations for several isomers of $C_{60}(C_2F_5)_4O$ derived by replacing the CF_3 groups in the most stable $C_{60}(CF_3)_4O$ isomers with C_2F_5 groups and then re-optimizing. Some of these results are also shown in Figure 9. We also considered several isomers with only *four* substituents, three CF_3 groups and one OCF_3 group. For this series of isomers, both *p*-$C_6(CF_3)(OCF_3)$ and *o*-$C_6(CF_3)(OCF_3)$ hexagons were considered along with a *p*-$C_6(CF_3)_2$ hexagon. Ten of these are also listed in Table S-1.

Discussion

The SPP Addition Pattern of C_s-$C_{60}(CF_3)_6$. In 2003, we reported that the reaction of C_{60} and $Ag(CF_3CO_2)$ at 280 °C, followed by sublimation of the $C_{60}(CF_3)_n$ products at 500 °C, produced a single abundant isomer of the first three members of the series, 1,7-$C_{60}(CF_3)_2$, C_1-*pmp*-$C_{60}(CF_3)_4$, and either C_1-*pmpmp*- or C_1-p^3*mp*-$C_{60}(CF_3)_6$.[20] Quantum chemical calculations showed that C_1-p^3*mp*-$C_{60}(CF_3)_6$ (the Schlegel diagram for which is shown in Figure 1) is 6.5 kJ mol^{-1} more stable than the C_1-*pmpmp* isomer and 14.4 kJ mol^{-1} more stable than the SPP C_s-$C_{60}(CF_3)_6$ isomer at the DFT level.[21] In 2003, the Sussex group reported that the same reaction without high-temperature sublimation led to 13 isomers of $C_{60}(CF_3)_6$, none of which were assigned to the SPP structure.[63] However, the room-temperature

(58) Creegan, K. M.; Robbins, J. L.; Robbins, W. K.; Millar, J. M.; Sherwood, R. D.; Tindall, P. J.; Cox, D. M.; Smith, A. B., III; McCauley, J. P., Jr.; Jones, D. R.; Gallagher, R. T. *J. Am. Chem. Soc.* **1992**, *114*, 1103−1105.
(59) Raghavachari, K. *Chem. Phys. Lett.* **1992**, *195*, 221−224.
(60) Raghavachari, K.; Sosa, C. *Chem. Phys. Lett.* **1993**, *209*, 223−228.
(61) Weisman, R. B.; Heymann, D.; Bachilo, S. M. *J. Am. Chem. Soc.* **2001**, *123*, 9720−9721.
(62) Wang, B. C.; Chen, L.; Chou, Y. M. *J. Mol. Struct. (Theochem)* **1998**, *422*, 153−158.
(63) Darwish, A. D.; Abdul-Sada, A. K.; Avent, A. G.; Lyakhovetsky, V. I.; Shilova, E. A.; Taylor, R. *Org. Biomol. Chem.* **2003**, *1*, 3102−3110.

^{19}F NMR spectrum of one of those 13 isomers (recorded in chloroform-*d*; see Figure 11 in the Sussex paper[63]) is, with two exceptions that can be easily explained, virtually identical to the 20 °C spectrum of C_s-$C_{60}(CF_3)_6$ shown in Figure 6. The first exception is that all of the chloroform-*d* δ values are shifted ca. 1.5 ppm to less negative values relative to our toluene-d_8 values. This chloroform-*d* vs toluene-d_8 shift in δ values has been observed for many other PFAFs we have examined. The second exception is that a combination of low signal/noise ratio and less than ideal phasing of the spectrum caused the Sussex group to mistake the apparent dectet with splittings of 11 Hz (at δ −59.9 in toluene-d_8 and δ −58.4 in chloroform-*d*) for an apparent septet.[63]

Our assignment of the SPP structure to C_s-$C_{60}(CF_3)_6$ is based on three lines of evidence. The first is that its electronic spectrum is similar to those of two other compounds with electron-withdrawing groups and the SPP structure, C_s-$C_{60}Cl_6$ and C_s-$C_{60}(CF_3)_4O$, as shown in Figure 8. The second is that its APCI mass spectrum exhibits a strong signal for the $C_{60}(CF_3)_5^-$ fragment ion in addition to the $C_{60}(CF_3)_6^-$ molecular ion, whereas the APCI mass spectrum of C_1-$C_{60}(CF_3)_6$, recorded under identical conditions, exhibits only the $C_{60}(CF_3)_6^-$ molecular ion, as shown in Figure 2. Facile loss of the CF_3 group attached to C1 in the SPP C_s-$C_{60}(CF_3)_6^-$ radical molecular ion is expected since it would produce the stable, closed-shell, cyclopentadienide-like C_{5v}-$C_{60}(CF_3)_5^-$ ion. The Schlegel diagram for the stable and structurally characterized[9,64] C_{5v}-$C_{60}Ph_5^-$ ion is also shown in Figure 2.

The third and most compelling line of evidence is an analysis of the ^{19}F NMR spectra (Figure 6) combined with DFT calculations. The 1:1:2:2 intensity pattern for the four multiplets requires time-averaged C_s symmetry, with the single-intensity CF_3 groups attached to cage C atoms that lie on the symmetry plane. The presence of time-averaged J_{FF} coupling of ca. 11−13 Hz between CF_3 groups requires that any pair of coupled CF_3 groups is attached to a shared hexagon. This conclusion is supported by the fact that observable coupling (of 8−16 Hz) between CF_3 groups in the structurally characterized PFAFs C_1-*pmp*^{3}*mpmp*-$C_{60}(CF_3)_{10}$,[25] C_1-p^3*mpmp*-$C_{60}(CF_3)_{10}$,[25,29] C_2-[p^3m^2-loop)]^2-$C_{60}(CF_3)_{10}$ (see Schlegel diagram in Figure 1),[30] C_s-$C_{70}(CF_3)_8$,[33,34] C_1-$C_{70}(CF_3)_{10}$,[25,35] and two isomers of C_1-$C_{70}(CF_3)_{12}$[36,37] is exhibited *only* by pairs of CF_3 groups that share a given fullerene hexagon (i.e., observable J_{FF} coupling has not been observed between CF_3 groups on different hexagons). The variable-temperature behavior of the δ −59.9 and −61.4 multiplets requires that their respective CF_3 groups have a higher barrier to rotation about their C−CF_3 bonds than the two pairs of symmetry-related CF_3 groups and therefore must be *ortho* to one another. This conclusion is based on the fact that none of the structurally characterized PFAFs just listed exhibit any peak broadening (the hallmark of hindered rotation) in the same temperature range (and this includes a pair of CF_3 groups on the 1 and 3 positions of a shared pentagon in C_1-*pmp*^{3}*mpmp*-$C_{60}(CF_3)_{10}$), and on the fact that the structurally characterized C_s and C_1 isomers of $C_{60}F_{17}(CF_3)$, which have one and two *o*-$C_6F(CF_3)$ hexagons, respectively,[65] exhibit not only CF_3 multiplet broadening at room temperature but also slow-exchange ^{19}F CF_3 multiplets at −50 and −30 °C, respectively.[66] The DFT-predicted C−CF_3 rotation barriers (i.e., $\Delta H^{\ddagger}$) for C_s- and C_1-$C_{60}F_{17}(CF_3)$ are 44 and 54 kJ mol^{-1}.[66] These values are probably reliable to within a few kilojoules per mole, because the experimental Eyring-plot-determined and DFT-predicted $\Delta H^{\ddagger}$ barriers to C−CF_3 rotation for the related compound *o*-$C_{60}F(CF_3)$ (i.e., 1,9-$C_{60}F(CF_3)$) are 46.8(7) and 46 kJ mol^{-1}, respectively. We have optimized the geometry of SPP C_s-$C_{60}(CF_3)_6$ at the DFT level, and the relevant part of this structure is shown in Figure 10. The DFT-predicted $\Delta H^{\ddagger}$ barriers to

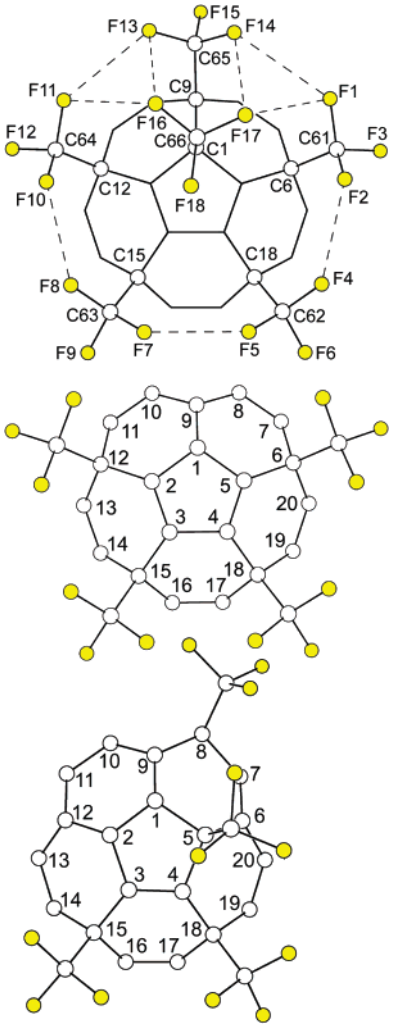

Figure 10. (Top) Part of the DFT-optimized structure of C_s-$C_{60}(CF_3)_6$, showing only the skew-pentagonal-pyramid portion of the molecule bearing the six CF_3 groups. Selected C−C distances are listed in Table 2. Other selected interatomic distances (Å): F1···F14, 2.695; F1···F17, 2.971; F2···F4, 2.683; F5···F7, 2.584; F8···F10, 2.654; F11···F13, 2.835; F11···F16, 2.753; F13···F16, 2.582; F14···F17, 2.573. (Middle) Part of the DFT-optimized structure of C_s-p^3-$C_{60}(CF_3)_4$. Selected interatomic distances (Å): C1−C9, 1.375; C2−C3, 1.378; C2−C12, 1.514; C12−C13, 1.541; C13−C14, 1.379; C16−C17, 1.380. (Bottom) Part of the DFT-optimized structure of C_1-*pmp*-$C_{60}(CF_3)_4$. Selected interatomic distances (Å): C1−C9, 1.382; C3−C4, 1.361; C4−C18, 1.518; C6−C7, 1.377; C7−C8, 1.516; C8−C9, 1.543; C16−C17, 1.376 Å; C17−C18, 1.545 Å; C18−C19, 1.542 Å. For convenience, the C atoms in the middle and bottom drawings have the same numbers as in the structure of C_s-$C_{60}(CF_3)_4O$, not the numbers that would give the lowest locants for the CF_3 groups. In all three drawings the smaller, highlighted circles are F atoms.

(64) Herber, R. H.; Nowik, I.; Matsuo, Y.; Toganoh, M.; Kuninobu, Y.; Nakamura, E. *Inorg. Chem.* **2005**, *44*, 5629−5635.
(65) Boltalina, O. V.; Hitchcock, P. B.; Troshin, P. A.; Street, J. M.; Taylor, R. *J. Chem. Soc., Perkin Trans. 2* **2000**, 2410−2414.
(66) Kareev, I. E.; Santiso Quinones, G.; Kuvychko, I. V.; Khavrel, P. A.; Ioffe, I. N.; Goldt, I. V.; Lebedkin, S. F.; Seppelt, K.; Strauss, S. H.; Boltalina, O. V. *J. Am. Chem. Soc.* **2005**, *127*, 11497−11504.

C−CF_3 rotation for the C65 and C66 CF_3 groups are 28 and 29 kJ mol^{-1}, which explains why these multiplets broaden and decoalescence below 20 °C but do not reach the slow-exchange limit (or even the near-slow-exchange limit) at −80 °C. For comparison, the DFT-predicted barriers for the unknown compound 1,9-$C_{60}(CF_3)_2$ and the known[20,63] compound 1,7-$C_{60}(CF_3)_2$ are 32 and 15 kJ mol^{-1}, respectively. Furthermore, C_s symmetry requires that the *ortho* CF_3 groups span a 6/6 junction and not a 5/6 junction.

Therefore, the isomer of C_s-$C_{60}(CF_3)_6$ that produced the NMR spectra in Figure 6 has an *ortho* pair of CF_3 groups on a 6/6 junction, a pair of symmetry-related CF_3 groups *meta* and *para* (but not *ortho*) to the 6/6 junction CF_3 groups, and another pair of symmetry-related CF_3 groups that share a hexagon with each other and with the first symmetry-related pair. The SPP addition pattern is the *only* addition pattern for C_s-$C_{60}(CF_3)_6$ that meets all of these criteria. Finally, we note that C_s-$C_{60}(CF_3)_6$ is much less abundant than C_1-$C_{60}(CF_3)_6$ in the 550 °C reaction products. If we accept the difference in DFT-predicted $\Delta H_f°$ values for the C_1 and C_s isomers of $C_{60}(CF_3)_6$, 14.4 kJ mol^{-1}, and if we account for the difference in symmetry numbers that favors the formation of the lower-symmetry C_1 isomer, 4.7 kJ mol^{-1} at 550 °C, the difference in $G_f°$ values at the reaction temperature is 19.1 kJ mol^{-1}. The mole ratio of the two compounds, *if* they were in thermal equilibrium at 550 °C (and this has not yet been proven for any pair of PFAFs at high temperature), would be 16:1, a value that is qualitatively consistent with the HPLC integrated peak intensities.

We note that C_s-$C_{60}(CF_3)_6$ is one of only 13 compounds in the chemical literature with sufficiently slow rotation about an element−CF_3 bond to exhibit an ^{19}F NMR spectrum that is not in the fast-exchange limit at any temperature lower than or equal to 20 °C.[66]

Where Are the σ and π Bonds? Any attempt to understand the thermodynamic and/or kinetic stability of a given fullerene-$(X)_n$ addition pattern will have to include an analysis of the remaining cage C−C σ and π bonds. The most straightforward *experimental* parameter that can be used to gauge relative bond strength (and hence relative bond order) is the C−C distance. The precision of fullerene X-ray structures (i.e., the estimated standard deviation, σ, for individual cage C−C bonds) has improved dramatically in the 3 years since Neretin and Slovokhotov's comprehensive review of over 400 fullerene structures was written.[67] In favorable cases, it is now possible to determine potentially important *and statistically significant* variations in C−C distances for different compositions or for different isomers of a given composition.

Furthermore, it is important to know if a particular computational method can be trusted with a sufficient degree of confidence to give accurate bond distances and angles in the absence of a crystal structure or when σ is too large. In order to confirm that the DFT code that we use gives meaningful bond distances for PFAFs, we compared the DFT-predicted cage C−C distances for C_1-p^3*mpmpmp*-$C_{60}(CF_3)_{10}$ (i.e., 1,6,11,16,-18,26,36,44,48,58-$C_{60}(CF_3)_{10}$, or $C_{60}(CF_3)_{10}$-2) with the distances determined by X-ray crystallography.[29] This particular compound was chosen for the comparison (i) because it is asymmetric, providing a comparison of 90 unique cage C−C bonds in one compound, and (ii) because it is one of the most precisely determined fullerene X-ray structures (σ values for individual cage C−C bonds range from 0.0014 to 0.0016 Å).[29] A plot of X-ray vs DFT distances for this compound is shown in the top panel in Figure 11. The agreement between the experimental and calculated C−C distances is excellent; the largest difference is less than 6σ, and most of the differences are 3σ or less.

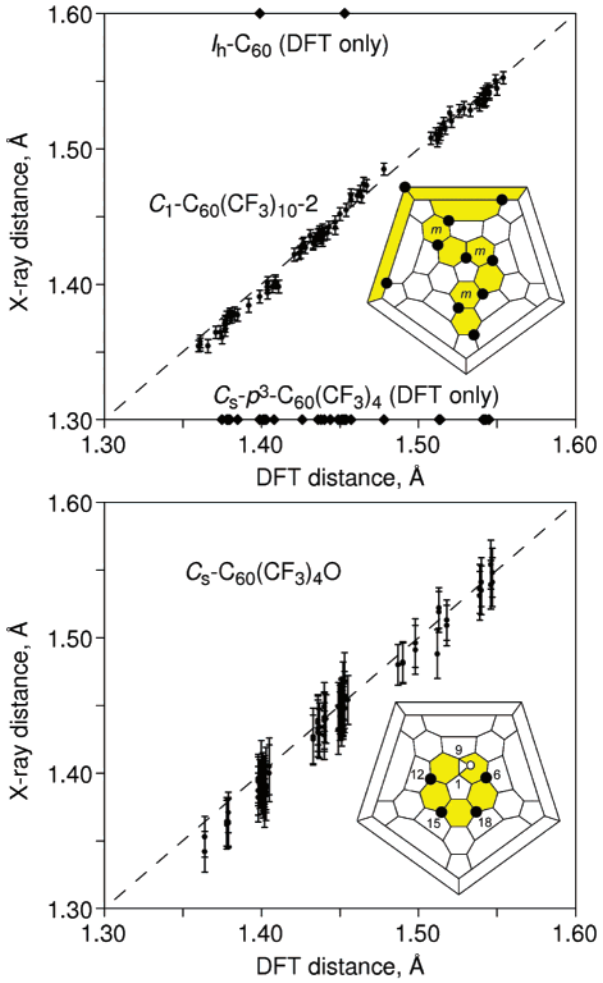

Figure 11. (Top) Plot showing the correlation between the 90 X-ray-derived and DFT-predicted cage C−C distances in C_1-p^3*mpmpmp*-$C_{60}(CF_3)_{10}$ (C_1-$C_{60}(CF_3)_{10}$-2; the error bars shown are ±3σ). Also shown on the top and bottom horizontal axes are the two DFT-predicted cage C−C distances in C_{60} and the 46 unique DFT-predicted cage carbon−carbon distances in C_s-p^3-$C_{60}(CF_3)_4$. (Bottom) Plot showing the correlation between the 90 X-ray-derived and 46 DFT-predicted cage C−C distances in C_s-$C_{60}(CF_3)_4O$ (the error bars shown are 3σ).

The top panel in Figure 11 also displays the two unique DFT-predicted distances for I_h-C_{60}, 1.399 Å for all 30 6/6 junctions (i.e., $C(sp^2)$−$C(sp^2)$ *double* bonds) and 1.453 Å for all 60 5/6 junctions (i.e., $C(sp^2)$−$C(sp^2)$ *single* bonds). In the most precisely determined structure of C_{60}, these two types of cage C−C bonds span the very narrow ranges (only 5σ) of 1.379(3)−1.391(3) and 1.447(3)−1.461(3) Å, respectively.[68] In contrast, the cage C−C bond distances in C_1-$C_{60}(CF_3)_{10}$-2 vary from 1.3545(14) to 1.5525(15) Å (more than 60 × 0.003 Å). Even the $C(sp^2)$−$C(sp^2)$ distances vary from 1.3545(14)

(67) Neretin, I. S.; Slovokhotov, Y. L. *Russ. Chem. Rev.* **2004**, *73*, 455−486.

(68) Olmstead, M. M.; de Bettencourt-Dias, A.; Lee, H. M.; Pham, D.; Balch, A. L. *Dalton Trans.* **2003**, 3227−3232.

to 1.4850(15) Å. The range is almost as broad in a fullerene-$(CF_3)_n$ compound with only four substituents, the putative compound C_s-p^3-$C_{60}(CF_3)_4$, as also shown in Figure 11. These broad ranges of $C(sp^2)-C(sp^2)$ distances mean that the labeling of cage $C(sp^2)-C(sp^2)$ bonds in exohedral fullerene *derivatives* as simply "single bonds" or "double bonds" is only meaningful as a first approximation. There is a continuous range of $C(sp^2)-C(sp^2)$ π bond orders in fullerene$(X)_n$ compounds.

No symmetry was imposed on the DFT structure of C_s-$C_{60}(CF_3)_4O$, but it adopted rigorous C_s symmetry upon optimization. In contrast, as shown in Table 2, the DFT structure of C_s-$C_{60}(C_2F_5)_4O$ optimized to idealized C_s symmetry, not rigorous C_s symmetry. The bottom panel in Figure 11 shows the correlation between the X-ray and DFT-predicted C−C distances for C_s-$C_{60}(CF_3)_4O$. In this case the agreement is also good, but the larger σ values for this X-ray structure (±0.005−0.007 Å, 3 times larger than for $C_{60}(CF_3)_{10}$-2) do not allow a distinction to be made among the shortest C−C bonds at the 99+% confidence level (i.e., $\pm 3\sigma$). Nevertheless, the DFT results predict that the isolated *cis*-butadiene fragment (C2−C3−C4−C5) has the two shortest C−C bonds in the molecule, at 1.364 Å. Note that these are 5/6 double bonds, which are normally considered to be destabilizing in [60]fullerene derivatives. However, the addition of any two substituents to the *para* C atoms of a given [60]fullerene hexagon always creates one double bond in a pentagon, so this is unavoidable in ribbon structures with p^3 and *pmp* sequences. The perimeter of the corannulene fragment that bears the substituents in C_s-$C_{60}(CF_3)_4O$ has the five next shortest C−C bonds (1.378 or 1.379 Å), and these five bonds, as well as the C−C bonds that range from 1.398 to 1.405 Å, are all 6/6 junctions. The longest 5/6 $C(sp^2)-C(sp^2)$ bond is 1.487 Å for C3−C4, which is the central C−C bond in the isolated *cis*-butadiene fragment. All of the remaining $C(sp^2)-C(sp^2)$ bonds in the DFT structure of C_s-$C_{60}(CF_3)_4O$, which range from 1.433 to 1.455 Å, are 5/6 junctions.

Comparison of SPP Structures. There are now a sufficient number of X-ray and DFT structures of fullerene derivatives with the $C_{60}X_6$ or $C_{60}X_4O$ SPP structures to allow them to be compared. Figure S-8 (Supporting Information) shows the DFT and/or X-ray C1−C9, C2−C3, and C4−C5 distances for $C_{60}Br_6$, $C_{60}(CH_3)_6$, C_s-$C_{60}(CF_3)_4O$, C_s-$C_{60}(C_2F_5)_4O$, and an isomer of $C_{60}(CF_3)_{10}$ that also has an isolated *cis*-butadiene fragment (the Schlegel diagram for the latter compound is shown in Figure 1). Interestingly, there is virtually no effect on the *cis*-butadiene fragment on changing the substituents from CH_3 to Br to CF_3, or on changing the C1 and C9 substituents from a pair of CH_3, Br, or CF_3 groups to an epoxide O atom, or on removing the C1 and C9 substituents entirely (as in $C_{60}(CF_3)_{10}$-4). On the other hand, the C1−C9 single-bond distance is quite sensitive to the nature of the substituent(s) to which they are bonded (or to the absence of substituents). The DFT-predicted distances for this bond vary by more than 0.1 Å for these six compounds. The lack of an effect on the C2−C3 and C4−C5 distances and the considerable effect on the C1−C9 distances strongly suggest that the changes in the latter are due to steric hindrance and not a substituent-based electronic factor.

Relative Energies of $C_{60}(R_f)_4O$ Isomers. In order to make this part of the Discussion easier to follow, the IUPAC cage numbering scheme used for C_s-$C_{60}(CF_3)_4O$ and C_s-$C_{60}(C_2F_5)_4O$ will also be used for C_s-p^3-$C_{60}(CF_3)_4$ and C_1-*pmp*-$C_{60}(CF_3)_4$. Fragments of the DFT-optimized structures of these two PFAF ribbon isomers are shown in Figure 10.

Figure 9 shows the nine lowest-energy ether (oxahomo[60]-fullerene) or epoxide (oxireno[60]fullerene) isomers of $C_{60}(CF_3)_4O$. Seven of them are conceptually derived by adding an O atom to a cage C−C double bond or by inserting an O atom into a cage C−C single bond of either C_s-p^3-$C_{60}(CF_3)_4$ or C_1-*pmp*-$C_{60}(CF_3)_4$. Only two of the nine isomers are derived from isomers of $C_{60}(CF_3)_4$ with two isolated $C_6(CF_3)_2$ hexagons. The nine isomers include two 5/6 epoxides (the 0.0 and 4.3 kJ mol^{-1} isomers), three 6/6 epoxides (the 5.6, 6.4, and 9.8 kJ mol^{-1} isomers), three 5/6 ethers (the 5.0, 6.8, and 9.1 kJ mol^{-1} isomers), and one 6/6 ether (the 8.2 kJ mol^{-1} isomer).

The relative stabilities of $C_{60}(CF_3)_4O$ epoxides appear to depend to a large extent on the placement of the O atom in a straightforward manner. The most stable isomers are those in which the O atom has been added to one of the shortest double bonds in the $C_{60}(CF_3)_4$ precursor. In C_s-p^3-$C_{60}(CF_3)_4$, the four shortest C−C bonds, which are proximate to the p^3 ribbon, are C1−C9 (1.375 Å), C16−C17 (1.375 Å), C2−C3/C4−C5 (1.378 Å), and C13−C14/C19−C20 (1.379 Å), and epoxidation of them produces the 5.6, 9.8, 0.0, and 6.4 kJ mol^{-1} isomers, respectively, in Figure 9. In C_1-*pmp*-$C_{60}(CF_3)_4$, the four shortest C−C bonds, which are proximate to the *pmp* ribbon, are C6−C7 (1.377 Å), C3−C4 (1.361 Å), C16−C17 (1.376 Å), and C1−C9 (1.382 Å), and epoxidation of them produces the four most stable *pmp* epoxides, the 4.3 kJ mol^{-1} isomer in Figure 9 and three isomers not shown in Figure 9 with relative $\Delta H_f°$ values of 11.9, 14.6, and 17.0 kJ mol^{-1}, respectively. The formation of a bis(epoxide) with O atoms formally added to the presumably very short double bonds of the isolated *cis*-butadiene fragment in SPP C_s-$C_{60}Me_5(OH)$ to form C_s-$C_{60}(CH_3)_5(OH)O_2$ has been reported.[52] In contrast, adding an O atom to the remote double bond, such as the 1.401 Å C52−C60 bond of C_1-*pmp*-$C_{60}(CF_3)_4$, produced a 6/6 epoxide isomer of $C_{60}(CF_3)_4O$ with a relative $\Delta H_f°$ value of 42.2 kJ mol^{-1}.

As far as 5/6 ethers are concerned, several isomers appear to be as stable as the most stable epoxides, and these are isomers in which the O atom has been inserted into a $C(sp^3)-C(sp^2)$ bond in the hypothetical $C_{60}(CF_3)_4$ precursor. This is sensible because these single bonds, which are greater than or equal to 1.52 Å in length, are appreciably longer and presumably weaker than typical fullerene 5/6 $C(sp^2)-C(sp^2)$ bonds, which are generally 1.45 ± 0.01 Å in length. Note that one of the DFT-predicted nine most stable structures shown in Figure 9 is a 6/6 ether (the 8.2 kJ mol^{-1} isomer), even though [61]oxahomofullerene 6/6 ethers are generally not stable. In fact, the 6/6 ether isomer with the O atom inserted into the C1−C9 bond of C_s-p^3-$C_{60}(CF_3)_4$ was transformed into the X-ray-diffraction-characterized epoxide C_s-$C_{60}(CF_3)_4O$ during DFT optimization.

In two cases, an ether and an epoxide with their respective O atoms bonded to the same numbered C atom are among the most stable isomers shown in Figure 9 and therefore are virtually equienergetic. They are the 4.3 and 8.2 kJ mol^{-1} isomers (a 5/6 epoxide and a 6/6 ether, respectively; the common bond is C7−O) and the 6.4 and 5.0 isomers (a 6/6 epoxide and a 5/6 ether, respectively; the common bond is C12−O). It will be interesting to see, in future computational work, if the activation energy for either isomerization is significantly different than

the DFT-predicted 175 kJ mol^{-1} activation energy for the isomerization of 6/6 epoxide-$C_{60}O$ to 5/6 ether-$C_{60}O$.[69]

Interestingly, we also found that many ether isomers of a different kind are up to 52 kJ mol^{-1} more stable than the most stable isomer shown in Figure 9. These are the trifluoromethoxytris(trifluoromethyl) isomers, $C_{60}(OCF_3)(CF_3)_3$, and the relative $\Delta H_f°$ values for 10 of them are listed in Table S-1. Since the OCF_3 group has an additional torsional degree of freedom compared to the CF_3 group, several isomers with *o*-$C_6(OCF_3)(CF_3)$ hexagons were among the most stable. However, the p^3 ribbon isomer with the OCF_3 group at one terminus of the ribbon was the most stable, just as the isomer C_s-p^3-$C_{60}(CF_3)_4$ is the most stable isomer of $C_{60}(CF_3)_4$.[21]

The most stable conformations of the C_2F_5 isomers shown in Figure 9 have about the same relative energies as the CF_3 isomers. There are four possible low-energy conformers for an isolated [60]fullerene *p*-$C_6(C_2F_5)_2$ hexagon (two are degenerate). Each CF_3 moiety can be situated over an adjacent pentagon or an adjacent hexagon. In the model compound 1,7-$C_{60}(C_2F_5)_2$, our DFT calculations show that these conformers vary in energy by only 1.6 kJ mol^{-1}. In the X-ray structure of C_1-*p,p,p*-$C_{60}(C_2F_5)_6$, which has three isolated *p*-$C_6(C_2F_5)_2$ hexagons, four of the C_2F_5 groups have their CF_3 moieties over adjacent hexagons and two have their CF_3 moieties over adjacent pentagons,[32] in harmony with this DFT prediction. On the other hand, in a compound with a ribbon of *m*- or *p*-$C_6(C_2F_5)_2$ edge-sharing hexagons, such as the X-ray-diffraction-characterized derivative C_1-p^3mp,*p*-$C_{60}(C_2F_5)_8$,[32] the interior C_2F_5 groups always have their CF_3 moieties over adjacent pentagons. This is also true for the two interior C_2F_5 groups in the structure of C_s-$C_{60}(C_2F_5)_4O$ (see Figure 4). In this epoxide, the CF_3 moieties for the two terminal C_2F_5 groups happen to be over their adjacent hexagons, but the calculations show that the four possible low-energy conformations for the terminal C_2F_5 groups in this isomer vary in energy by only 4.5 kJ mol^{-1}.

Raman Spectra of C_s-$C_{60}(R_f)_4O$. (a) Cage Vibrations. The clustering of 50 of the 90 cage C−C distances at ca. 1.40 or at ca. 1.45 Å in the lower panel in Figure 11 shows that more than half of the fullerene cage in C_s-$C_{60}(CF_3)_4O$ is undistorted from C_{60}. Since the Raman spectra of most exohedral fullerene derivatives are dominated by cage vibrations, it is sensible to discuss the Raman spectra of C_s-$C_{60}(CF_3)_4O$ and C_s-$C_{60}(C_2F_5)_4O$ in terms of C_{60} normal modes using projection analysis.[70,71] Table S-2 (Supporting Information) lists the experimental and DFT-calculated Raman bands and their correlation to C_{60} normal modes (since the vibrations of the two compounds are so similar, the projection analysis in Table S-2 is limited to the case of $C_{60}(CF_3)_4O$). The spectra are shown in Figure 7.

The low-frequency range for each compound is characterized by a high vibrational density of states due to the partial mixing of vibrations of the CF_3 or C_2F_5 groups with cage normal modes. However, the Raman intensities of perfluoroalkyl groups are, in general, very weak, and these vibrations are observed only when mixed with the proper cage vibrations. An exception is a group of CCC deformations in the C_2F_5 groups in C_s-$C_{60}(C_2F_5)_4O$, which appear as an unresolved band at 145 cm^{-1}. In the 170−210 cm^{-1} range, the contribution of cage C atom displacements in the vibrations of both $C_{60}(R_f)_4O$ compounds appears to be less than 40%. However, a close analysis revealed that the cage deformations in these vibrations reproduce the displacements of the $H_g(1)$ normal modes of C_{60} (272 cm^{-1}),[72] along with radial displacements of the CF_3 or C_2F_5 groups (but without internal deformations of the latter). Thus, in spite of the low formal cage contributions, medium-intensity bands at 180 and 217 cm^{-1} for C_s-$C_{60}(CF_3)_4O$ and at 190, 195, and 212 cm^{-1} for C_s-$C_{60}(C_2F_5)_4O$ appear in this range. Intense bands at 253 and 269 cm^{-1} for C_s-$C_{60}(CF_3)_4O$ and at 258 and 268 cm^{-1} in C_s-$C_{60}(C_2F_5)_4O$ are due predominantly to cage vibrations that are derived from the C_{60} $H_g(1)$ modes. Finally, $H_g(1)$-derived cage deformations, mixed with internal CCF and FCF deformations, appear as weak- to medium-intensity bands in the 280−310 cm^{-1} range. Thus, vibrations that correlate with the C_{60} $H_g(1)$ normal modes are scattered in the 170−310 cm^{-1} range in the spectra of both $C_{60}(R_f)_4O$ compounds, endowing them with considerable Raman intensity.

Above 330 cm^{-1}, all of the Raman bands of $C_{60}(R_f)_4O$ with considerable intensity are presumably localized on the C_{60} cage. The weak bands at 330−370 cm^{-1} are correlated with the Raman-inactive $F_{2u}(1)$ and $G_u(1)$ modes of C_{60}. The bands at 421, 431, and 452 cm^{-1} for C_s-$C_{60}(CF_3)_4O$ and at 422, 430, and 452 cm^{-1} for C_s-$C_{60}(C_2F_5)_4O$ are correlated with the $H_g(2)$ modes of C_{60} at 432 cm^{-1} and are partially mixed with the Raman-inactive $G_g(1)$ fundamentals of C_{60}. The C_{60} $A_g(1)$ "breathing" vibration at 497 cm^{-1}, which is the third-most-intense band in the off-resonance or 1064-nm excitation Raman spectrum of C_{60},[73] correlates with the 475/494 cm^{-1} and 479/493 cm^{-1} doublets in the spectra of C_s-$C_{60}(CF_3)_4O$ and C_s-$C_{60}(C_2F_5)_4O$, respectively. A 10% contribution of the $A_g(1)$ C_{60} mode plus a ca. 40% contribution from the Raman-inactive C_{60} $F_u(1)$ modes gives rise to the medium-intensity bands at 566 and 553 cm^{-1} in C_s-$C_{60}(CF_3)_4O$ and C_s-$C_{60}(C_2F_5)_4O$, respectively. Finally, the band at 787 cm^{-1} in the spectra of both C_s-$C_{60}(R_f)_4O$ molecules is correlated with the $H_g(4)$ modes of C_{60} at 773 cm^{-1}.

The Raman spectra of $C_{60}(R_f)_4O$ resemble that of C_s-$C_{60}Cl_6$ in the range of tangential cage modes.[6] Projection analysis unambiguously shows that the strongest band in the entire spectrum of both molecules, 1465/1466 cm^{-1}, is strongly correlated with the C_{60} $A_g(2)$ fundamental. The much weaker band at 1441/1442 cm^{-1} is due to a combination of the nearly degenerate $H_g(7)$, $F_{1u}(4)$, and $G_u(6)$ normal modes of C_{60}. Finally, two partially resolved bands at 1569 and 1583 cm^{-1} are due to mixtures of the C_{60} $H_u(6)$ and $H_g(8)$ bands at 1567 and 1575 cm^{-1}.

(b) Vibrations of the Epoxy Group. In general, the characteristic vibrations of oxirane rings are found at 750−880 (the symmetric ring deformation), 815−950 (the antisymmetric ring deformation), and 1230−1280 cm^{-1} (the ring breathing vibration), the latter of which usually has considerable Raman intensity.[74] However, the vibrations of the oxirane ring in $C_{60}O$ could not be unambiguously assigned because of their low

(69) Xu, X.; Shang, Z.; Wang, G.; Cai, Z.; Pan, Y.; Zhao, X. *J. Phys. Chem. A* **2002**, *106*, 9284−9289.
(70) Popov, A. A.; Goryunkov, A. A.; Goldt, I. V.; Kareev, I. E.; Kuvychko, I. V.; Hunnius, W.-D.; Seppelt, K.; Strauss, S. H.; Boltalina, O. V. *J. Phys. Chem. A* **2004**, *108*, 11449−11456.
(71) Popov, A. A.; Senyavin, V. M.; Granovsky, A. A. *Chem. Phys. Lett.* **2004**, *383*, 149−155.
(72) Bethune, D. S.; Meijer, G.; Tang, W. C.; Rosen, H. J.; Golden, W. G.; Seki, H.; Brown, C. A.; de Vries, M. S. *Chem. Phys. Lett.* **1991**, *179*, 181−186.
(73) Lynch, K.; Tanke, C.; Menzel, F.; Brockner, W.; Scharff, P.; Stumpp, E. *J. Phys. Chem.* **1995**, *99*, 7985−7992.

intensities.[75] This appears to be true for the $C_{60}(R_f)_4O$ molecules as well. Our calculations predict that the oxirane ring breathing vibration should appear at 1375 cm^{-1}, but only very weak and broad bands were observed near this frequency. The other oxirane modes are predicted to be strongly mixed with cage vibrations. For example, the antisymmetric ring deformation is predicted to make a significant contribution to bands at 854 and 1068 cm^{-1}, and weak bands at 857 and 1078 cm^{-1} in the Raman spectrum of C_s-$C_{60}(CF_3)_4O$ can be tentatively assigned to this mode. A band with a significant contribution of the symmetric ring mode is predicted at 828 cm^{-1}, and this probably corresponds to the experimental Raman line at 848 cm^{-1}.

Summary. Three compounds that exhibit the SPP C_s-$C_{60}X_6$ or C_s-$C_{60}X_4O$ addition patterns are reported, two of which are new and one of which was previously reported but was incorrectly assigned. The epoxides are the first PFAF derivatives with non-fluorine-containing exohedral substituents known to be stable at temperatures exceeding 400 °C, indicating that perfluoroalkyl substituents can enhance the thermal stability of fullerene derivatives that have other substituents as well. They are also the first fullerene epoxides of any type that are stable at elevated temperatures. C_s-$C_{60}(CF_3)_6$ is the first [60]fullerene derivative with adjacent CF_3 groups, something that has not been observed in any of two dozen or so fullerene$(R_f)_n$ derivatives with $n = 1-14$ reported to date. The fact that it is stable at temperatures exceeding 500 °C is significant, given that the DFT-predicted $(CF_3)C-C(CF_3)$ distance exceeds 1.60 Å.

Acknowledgment. We appreciate the financial support from the Volkswagon Foundation (I-77/855), the Russian Federal Agency of Science and Innovations (Contract 02.442.11.7439), and the Colorado State University Research Foundation. We thank Professor Manfred Kappes for his continuing support, Donald L. Dick for assistance with APCI mass spectrometry, and Warren S. Powell and Carlo Thilgen for their advice and assistance regarding fullerene nomenclature. The authors dedicate this paper to Professor Karl O. Christe on the occasion of his 70th birthday.

Supporting Information Available: Figures showing the skew pentagonal-pyramid fragment of C_s-$C_{60}Br_6$ and the second-stage HPLC purification and additional structural drawings of C_s-$C_{60}(CF_3)_4O$ and C_s-$C_{60}(C_2F_5)_4O$; relative DFT-predicted $\Delta H_f°$ values isomers of $C_{60}(CF_3)_4O$ and for the four conformations of some isomers of $C_{60}(C_2F_5)_4O$; selected experimental and DFT-predicted Raman frequencies for C_s-$C_{60}(CF_3)_4O$ and C_s-$C_{60}(C_2F_5)_4O$ and their correlation with C_{60} normal modes; X-ray crystallographic data, in CIF format. This material is available free of charge via the Internet at http://pubs.acs.org.

JA063907R

(74) Lin-Vien, D.; Colthup, N.; Fateley, W.; Grasselli, J. *The Handbook of Infrared and Raman Characteristic Frequencies of Organic Molecules*; Academic Press: New York, 1991.
(75) Krause, M.; Dunsch, L.; Seifert, G.; Fowler, P. W.; Gromov, A.; Kratschmer, W.; Gutierez, R.; Porezag, D.; Frauenheim, T. *J. Chem. Soc., Faraday Trans.* **1998**, *94*, 2287−2294.